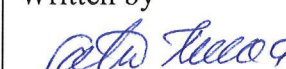
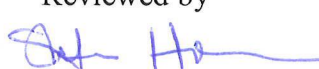
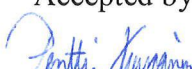


## Performance of superheater materials in simulated oxyfuel combustion

Authors: Satu Tuurna, Pekka Pohjanne, Pertti Auerkari

Confidentiality: Public



Report's title Performance of superheater materials in simulated oxyfuel combustion	
Customer, contact person, address Tekes	Order reference 40118/08 (593/31/08)
Project name High performance materials and corrosion control for efficient and low emission biomass and waste combustion, HICOR	Project number/Short name 26805
Author(s) Satu Tuurna, Pekka Pohjanne, Pertti Auerkari	Pages 37
Keywords Superheater, corrosion, oxyfuel, deposit	Report identification code VTT-R-02456-11
Summary  <p>This report describes the results of the project "High performance materials and corrosion control for efficient and low emission biomass and waste combustion" (HICOR, Tekes contract 40118/08) on corrosion testing at 600 and 650°C in gas atmospheres simulating oxyfuel combustion. The results are compared to corresponding results from simulated air firing conditions.</p> <p>Exposure testing was conducted on selected ferritic, austenitic and Ni-based materials. The results suggest that without added impurities like sulphur and chlorides, the simulated oxyfuel conditions do not result in more severe corrosion than the air firing environment. In more realistic oxyfuel case, flue gas recirculation would considerably increase the concentration of these impurities. Corrosion and microstructural changes like carburisation may also affect the damage mechanisms of boiler materials (e.g. creep, fatigue properties), and thus decrease the expected component life.</p> <p>No carburisation of the metal substrate was observed after exposure to simulated oxyfuel gas atmospheres without deposit, although some carbon enrichment was detected near the oxide-surface interface. With extended exposure time, the oxide scale properties may change to enable metal carburisation. The exposure with CaCO<sub>3</sub>-CaSO<sub>4</sub> deposit in 60% CO<sub>2</sub>-30% H<sub>2</sub>O-4% O<sub>2</sub>-Ar gas at 650°C resulted in corrosion of all tested alloys and clear carburisation of steels X20CrMoV11-1 and TP347HFG.</p>	
Confidentiality	Public
Espoo 21.6.2011 Written by  Satu Tuurna Senior scientist	
Reviewed by  Stefan Holmström Team leader	
Accepted by  Pentti Kauppinen Technology manager	
VTT's contact address P.O. Box 1000, 02044 VTT, kirjaamo@vtt.fi	
Distribution (customer and VTT) Project steering group, VTT archive	
<i>The use of the name of the VTT Technical Research Centre of Finland (VTT) in advertising or publication in part of this report is only permissible with written authorisation from the VTT Technical Research Centre of Finland.</i>	

## Preface

This report is based on the results from laboratory testing performed at VTT. The goal of the VTT part in the project was to estimate the oxidation/corrosion behaviour of selected alloys exposed to moist CO<sub>2</sub> rich simulated flue gas with and without CaCO<sub>3</sub>-CaSO<sub>4</sub> deposit at high temperatures relevant to oxyfuel combustion. The results of gas exposure testing without deposit were compared to corresponding results from simulated air-fired coal combustion conditions.

This work was a part of the HICOR project (Tekes contract 40118/08). The authors wish to thank Tekes, Fortum Oyj, Foster Wheeler Energy Oy and VTT for the financial and other support during the project.

Tampere, June 2011

Authors

## Contents

Preface .....	2
1 Introduction.....	4
2 Experimental.....	6
3 Results .....	7
3.1 Exposure testing under gas atmospheres.....	7
3.2 Exposure tests under CaCO <sub>3</sub> -CaSO <sub>4</sub> deposit at 650°C .....	11
4 Discussion and conclusions.....	15
5 Summary .....	18
References .....	19

## 1 Introduction

The energy sector is globally the largest CO<sub>2</sub> emitter, Fig. 1. Carbon capture and storage (CCS) is a concept to reduce greenhouse gas emissions resulting from the use of fossil fuels in power generation. Three main process alternatives have been suggested for extracting CO<sub>2</sub>:

- Pre-combustion concepts – fuel carbonization and subsequent burning of hydrogen
- Post-combustion concepts – tail-end carbon dioxide capture solutions such as amine scrubbing
- Integrated oxycombustion concepts – combustion is carried out in oxygen-enriched environment to make post-combustion extraction easier.

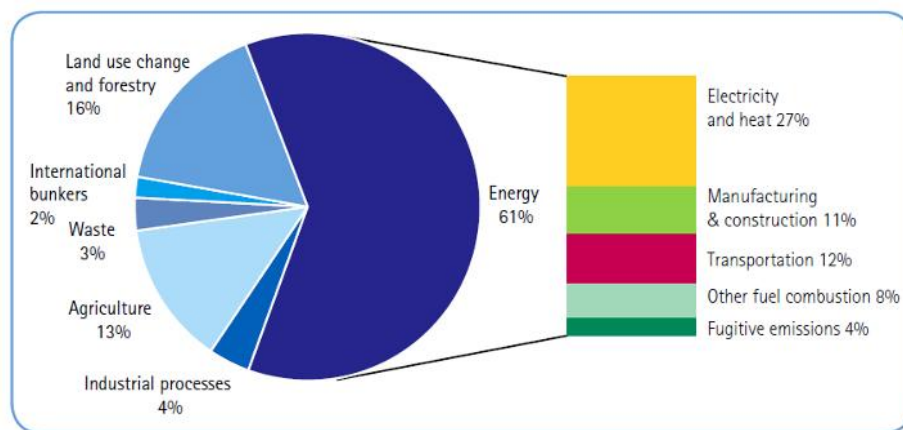


Figure 1. Global CO<sub>2</sub> emission sources [1].

In oxycombustion almost all atmospheric nitrogen is eliminated and the produced flue gas mainly consists of CO<sub>2</sub> and H<sub>2</sub>O with small amounts of O<sub>2</sub>, Ar, N<sub>2</sub> with some impurities like SO<sub>2</sub> and Cl. The first demonstrations of the oxyfuel concept are carried out with the current high temperature materials. The most critical components will be those in contact with the hot flue gas environment. The risk of enrichment of corrosive species in the flue gas environment strongly increases due to recycling of flue gas in oxy-fired combustion compared to air firing. Literature review also suggests that there will be higher amounts of sulphur in the ash under oxyfuel conditions. Typically the presence of sulphur strongly increases the corrosion rate, but the influence of sulphur on corrosion can be complicated, as in the form of SO<sub>2</sub> it can also slow down corrosion. The phenomenon is dependent on time, current environment, gas partial pressures and alloying elements [2-7]. Fig. 2 shows corrosion rates of different superheater materials under conventional and oxyfuel conditions in the presence of SO<sub>2</sub> [7]. It has been suggested that oxide scales developing in O<sub>2</sub>/CO<sub>2</sub>/H<sub>2</sub>O atmospheres are not well protective and internal carburisation may occur [4,8,9]. In oxyfuel combustion the possibility to the presence of sticky deposits are increased [10,11]. Sulphination and carbonation of ash particles under oxycombustion is higher due to high SO<sub>2</sub> and CO<sub>2</sub> potential. The CO<sub>2</sub>-rich environment could lead to more unburned carbon in the deposits, and insufficient attention to burner design could result in elevated CO concentrations. These conditions have been linked to locally reducing conditions below the ash, resulting in accelerated corrosion [4,12].



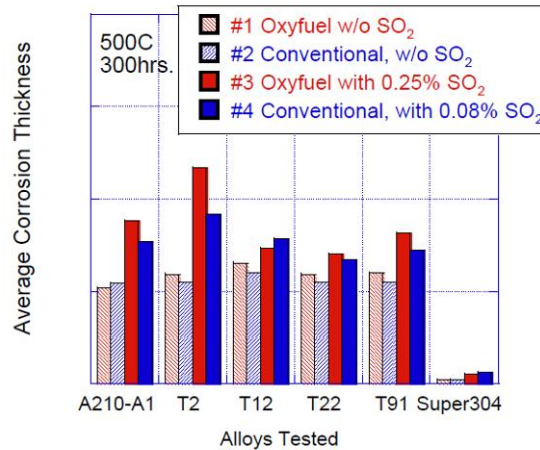


Figure 2. Gas corrosion test results after 300 h at 500°C from IHI, Japan [7].

Higher oxide scale growth under oxyfuel conditions was observed due to higher H<sub>2</sub>O content in studies of Stein-Brzozowska et al. [11]. It is well known that the high temperature oxidation rates can significantly increase in water containing environments [13,14]. It has also been suggested that the scale thickness is dependent on pressure of the gas mixture [11], and generally increasing pressure will result in thicker oxide scale [15]. Piron et. al [9] have suggested that in CO<sub>2</sub>- and/or H<sub>2</sub>O-rich gases, the steels P92, X20, VM12 and 13CrMo44 tend to form iron-rich oxide scales with significantly higher growth rates than with the Cr-rich surface scales formed during air exposure. The iron-rich oxide scales were explained as a result of a decreased flux of chromium in the bulk alloy towards the surface due to enhanced internal oxidation of chromium in the H<sub>2</sub>O-containing gases and carbide formation in the CO<sub>2</sub>-rich gases. Additionally, the presence of water vapour in the exposure atmosphere affected buckling of the outer hematite layer. The iron based oxide scales formed in CO<sub>2</sub>(-H<sub>2</sub>O)-rich gases are suggested to be permeable to CO<sub>2</sub> molecules resulting in substantial carburization of the steel. Hünert et al. [8,15] reported intensive carburisation of 2-12% Cr alloys at 550°C and higher temperatures. The carburisation was promoted by increasing Cr content until formation of a dense chromia layer. Carburisation was observed near the oxide-metal interface showing additional formation of Fe<sub>2</sub>C or pearlite phases. In general, it has been suggested that Cr steels oxidized in high CO<sub>2</sub>-containing gas mixtures are prone to carburization if poorly protective iron based oxide scales are formed [16,17]. Easier formation of Cr<sub>2</sub>O<sub>3</sub> scale on nickel or cobalt based alloys compared to iron based alloys protects these materials from carburisation. Grabke et al. [18] have also suggested that the carbon permeation through the oxide layers is caused by carbon containing gases diffusing via cracks, pores and other oxide scale defects. The carburization behaviour of the steels is dependent on temperature, pressure, and alloy and gas composition. Carburization and oxidation kinetics is shown to accelerate with the increase of pressure of corrosive gases [19]. More discussion of corrosion mechanisms and related thermodynamics in atmospheres containing CO<sub>2</sub> are pulled together in the report VTT-R-04861-11 [20].

The present report describes laboratory testing of selected alloys under simulated oxy- and air-fired combustion conditions. The samples are analysed in terms of weight change and surface structure in cross-section microscopy, EDS and GDOES.

## 2 Experimental

The test materials included four grades of typical boiler tube steels and two Ni-based alloys, Table 1. Rectangle shape specimens with dimensions of 12 x 18 x 3 mm were machined from thick walled tubes. The samples were bright polished with SiC paper (P1200) and ultrasonically degreased in ethanol. Two parallel samples were used in exposure testing.

The multi-sample exposure tests were carried out under isothermal conditions at temperatures of 600 and 650°C up to 1000 hours with and without deposit, and with gas compositions shown in Table 2. The used deposit contained 85 wt% CaCO<sub>3</sub> and 15 wt% CaSO<sub>4</sub>. All tests were carried out in horizontal tube furnaces, Fig. 3. The flow rate of gases was 10 l/h, controlled by mass-flow controllers. The carrier gas was passed through a humidifying unit containing deionised water before the furnace, to add moisture to the gas mixture. In tests with deposit, two thirds of the sample height was buried in the deposit, Fig. 3.

Table 1. Nominal compositions (in wt%) of the test materials

Alloy	Fe	Cr	Ni	Mo	Other
X20CrMoV11-1	bal.	11.2	0.5	0.8	0.49 Mn, 0.3 V, 0.26 Si, 0.2 C
TP347HFG	bal.	18.3	11.7	0.23	1.64 Mn, 0.92 Nb, 0.33 Cu, 0.4 Si, 0.07 C
TP347HFG(CN)	bal.	18.6	11.6	0.04	1.56 Mn, 0.77 Nb, 0.03 Cu, 0.4 Si, 0.07 C
HR3C	bal.	25.5	19.4	0.11	1.1 Mn, 0.39 Si, 0.45 Nb, 0.06 C
Sanicro 25	bal.	22.3	24.9	-	3.4W, 1.5Co, 2.9Cu, 0.5Nb, 0.2Si, 0.3Mn, 0.24N, 0.06C
A263	0.4	20.4	50.7	5.35	19.9 Co, 0.26 Mn, 0.23 Si, 0.5 Al, 2.3 Ti, 0.05 C
A617	1.1	22.9	52.4	9.19	12.67 Co, 0.1 Si, 1.17 Al, 0.44 Ti

Table 2. Test conditions for laboratory tests.

Simulated system	Vol.%					Temp. °C	Duration h
	N <sub>2</sub>	O <sub>2</sub>	CO <sub>2</sub>	H <sub>2</sub> O	Ar		
Air-fired	73.7	1.8	16.0	8.5	-	600, 650	168, 500, 1000
Oxyfuel	-	3.6	60.0	30.0	6.4		

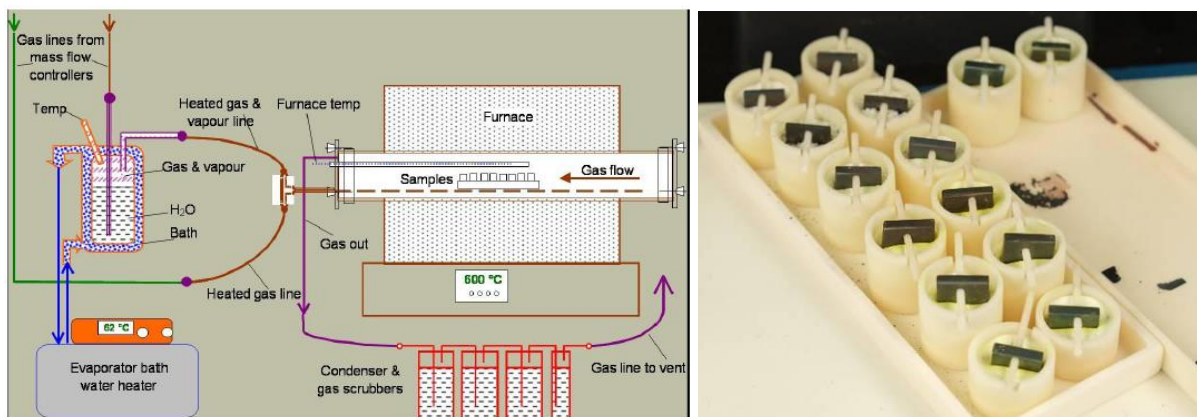


Figure 3. VTT furnace system for multi-sample exposures and sample placement in crucibles.



The sample cross-sections were studied with optical and scanning electron microscope (SEM). The composition of oxide layers was determined with energy dispersive spectroscopy (EDS). In addition, selected oxide scales were analysed with glow discharge optical emission spectroscopy (GDOES). In the case of tests with deposit, longitudinal cross-sections were inspected at two positions (under deposit and gas exposure only).

Assessment of material performance under selected environments was based on the estimation of the oxide layer thickness or/and depth of the material degradation. The thickness of oxide layers around the samples with 8 measurement points was determined under optical microscope. However, there was some spallation of the oxide layers during the exposure testing, and thus the measurement results are taken as indicative only. To monitor oxidation, weight (mass) change measurements of exposed samples were also carried out for the specimens without deposits. Spalled oxides were collected, when possible, and weighed with the samples.

### 3 Results

#### 3.1 Exposure testing under gas atmospheres

The exposure tests were performed at 600 and 650°C under simulated oxy- and air-fired combustion conditions up to 1000 h. Fig. 4 summarises the results in terms of weight change after exposure of 1000 h. The results represent the maximum weight change of duplicate samples. All measurement results are included in Appendix 1, and also in the summary report [21]. The oxidation rates of X20 and TP347HFG(CN) at 600°C were lower in the oxyfuel conditions than in the reference conditions of air-fired coal combustion. A similar trend was also observed in the alloys Sanicro 25 and HR3C, although the oxidation rates of these alloys were almost negligible. Compared to TP347HFG(CN) at 600°C, steel TP347HFG behaved rather similarly in air but showed higher weight change in the oxyfuel atmosphere. However, in many cases the weight changes were small (below 0.05 mg/cm<sup>2</sup>), therefore not implying definite conclusions at least alone. At 650°C steel X20 showed slightly more extensive oxidation after 1000 h in oxyfuel conditions than in reference air conditions. However, the opposite trend was observed for the other alloys. Table 3 summarises the results as oxide thickness on steels X20 and TP347HFG at 650°C. Only X20 exposed to oxyfuel conditions had a continuous oxide on the studied cross-section after 500 h of exposure; all other samples only showed some nodular oxides on the surfaces. The results of GDOES analyses of austenitic and Ni alloys indicated oxide film thickness below 1 µm, Appendix 2.

*Table 3. Mean oxide thickness [µm] on steels X20CrMoV11-1 (X20) and TP347HFG after exposure at 650°C; \* discontinuous nodular oxide*

Steel – gas environment	168 h	500 h	1000 h
X20 – air combustion	30*	35*	50
X20 – oxyfuel combustion	20*	45	55
TP347HFG – air combustion	10*	10*	30
TP347HFG – oxyfuel combustion	15*	10*	20

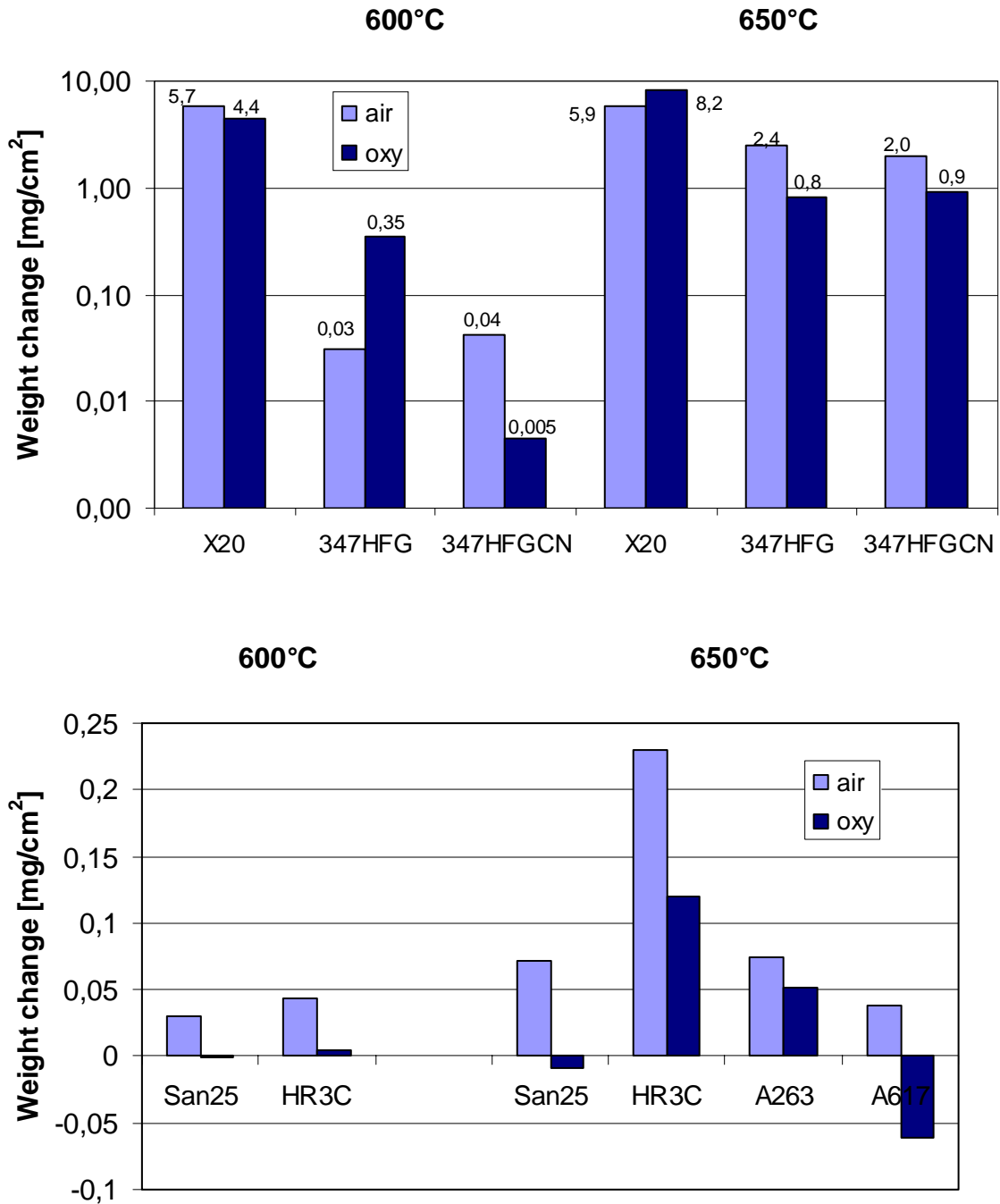


Figure 4. Weight gain [mg/cm<sup>3</sup>] of specimens exposed 1000 h to air and oxyfuel conditions at 600 and 650°C; note logarithmic (upper) and linear (lower) scales of the vertical axes.

The X20 samples showed oxide thickness of about 35-40  $\mu\text{m}$  after exposure at 600°C, Fig. 5, although there were parts of surface where no oxide was formed yet. These oxides consisted of two layers, an iron rich oxide growing outwards from original surface and an inwards growing iron-chromium spinel layer. Below the oxide there was a zone of internal oxidation that was more clearly apparent in the sample exposed under simulated oxyfuel conditions (Fig. 5b). The oxide film grown on TP347HFG was analysed with GDOES, and only a very thin oxide film, 0.2  $\mu\text{m}$ , could be observed after exposure at 600°C, Appendix 2.

The oxide formed on steel X20 at 650°C also had a two-layer structure, with an outer iron-rich layer and an inner porous mixed oxide of iron and chromium with minor amounts of other elements from the alloy, Fig 6. There were no significant structural differences between oxides formed in air and oxyfuel environments at 650°C. No internal oxidation zone was found beneath the oxide scale. Some carbon was found near the interface between inner and outer oxide layer, and also inside the inner oxide layer after 1000 h exposure to oxyfuel environment, Fig. 7.

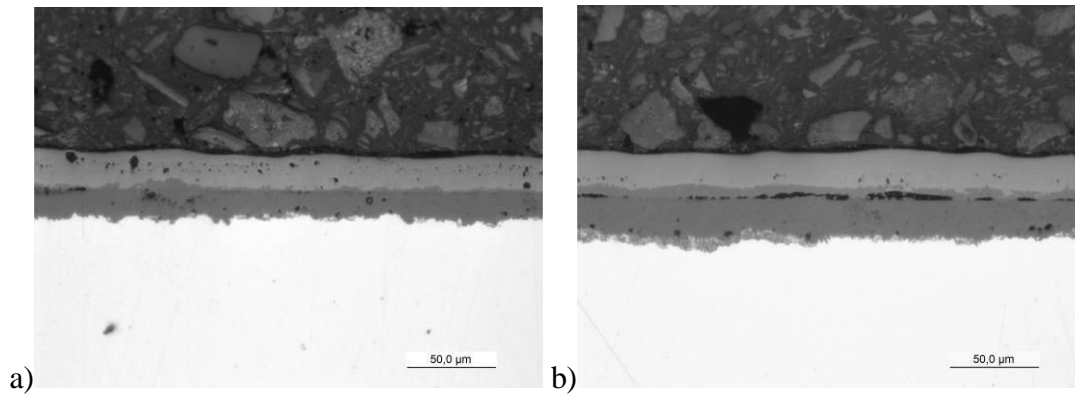


Figure 5. Oxide layers formed on X20 samples after 1000 h exposure at 600°C in a) air and b) oxyfuel environment.

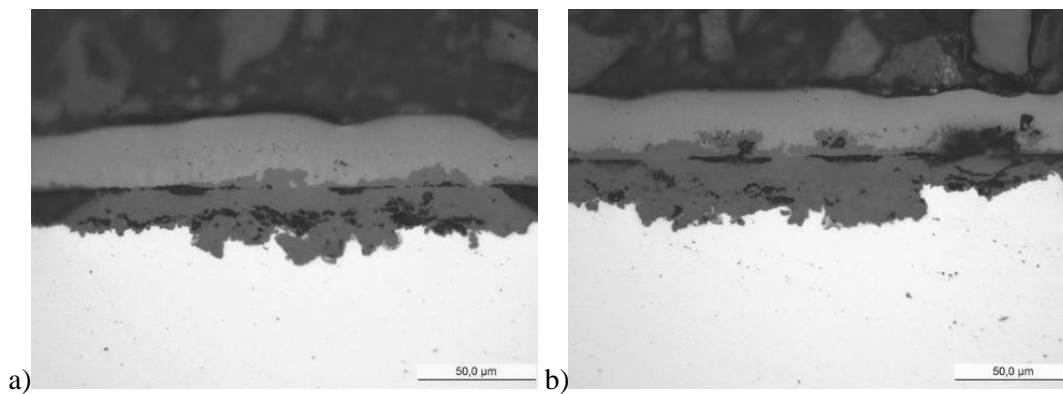


Figure 6. Oxide layers formed on X20 samples after 1000 h exposure at 650°C in a) air and b) oxyfuel environment.

With short exposure times (168 and 500 h), only very thin or no oxide scale formed on alloy TP347HFG at 650°C. After 1000 h exposure at 650°C in air combustion environment, a continuous two-layer oxide was observed. In contrast, the same steel showed uneven oxides with a nodule structure after corresponding exposure in oxyfuel environment; although locally a continuous scale was found in some parts of the sample, Fig. 8. EDS analyses showed an iron rich outer oxide layer and a mixed oxide inner layer mainly containing iron, chromium and nickel.

Comparing oxidation of TP347HFG and TP347HFG(CN), it was observed that the latter showed weaker adherence of oxide, with spallation of the outer oxide layer, Fig 9. For clarification, grain size and hardness of the samples was measured. The grain size of both materials were similar (8/100) but hardness for 215 HV5 for TP347HFG and 168 HV5 for TP347HFG(CN), suggesting differences in the degree of cold work.

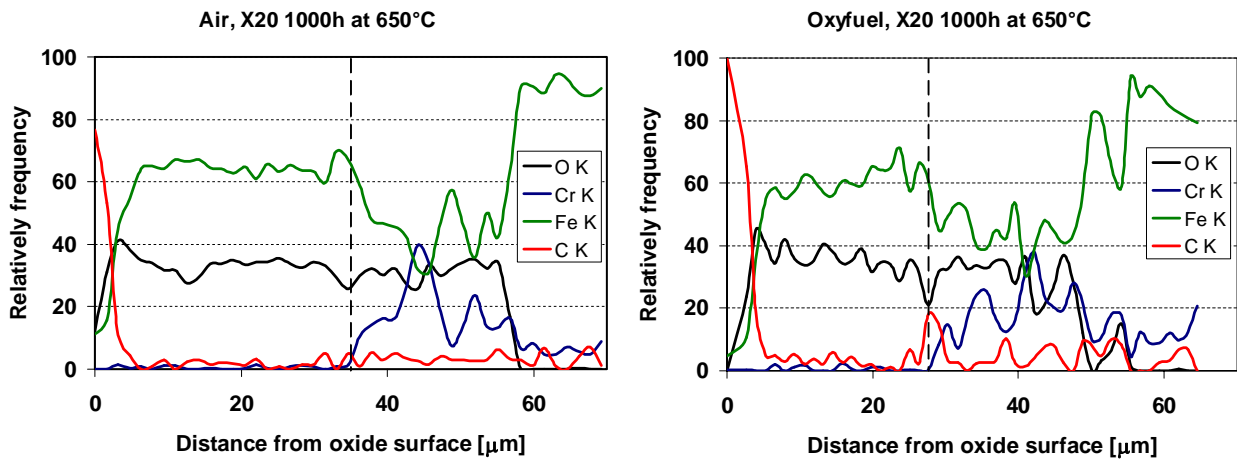


Figure 7. EDS line scan analyses across the oxides formed on X20 after 1000 h at 650°C in a) air and b) oxyfuel combustion environments; the dashed line represents the interface between outer and inner oxide layers (~original surface)

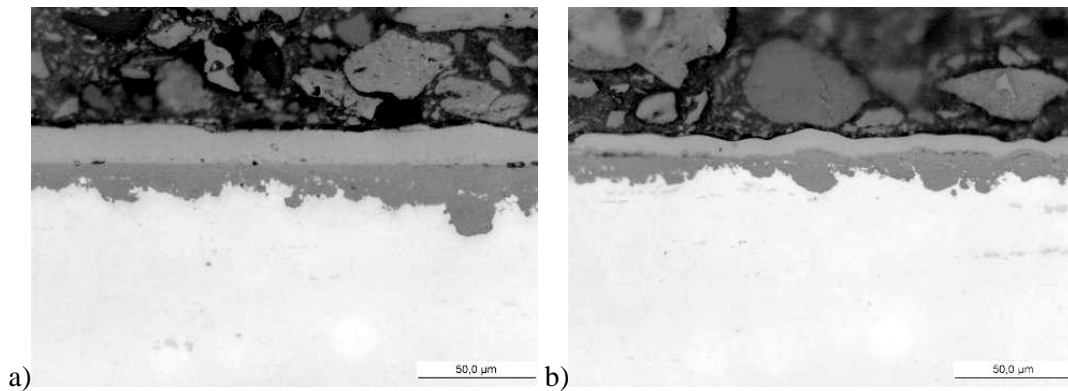


Figure 8. Oxide layers on TP347HFG after 1000 h exposure at 650°C in a) air combustion and b) oxyfuel combustion environment.

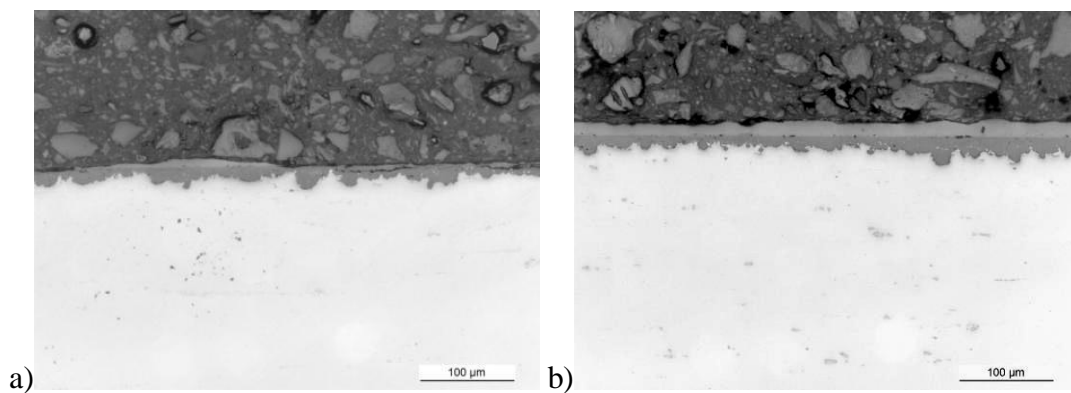
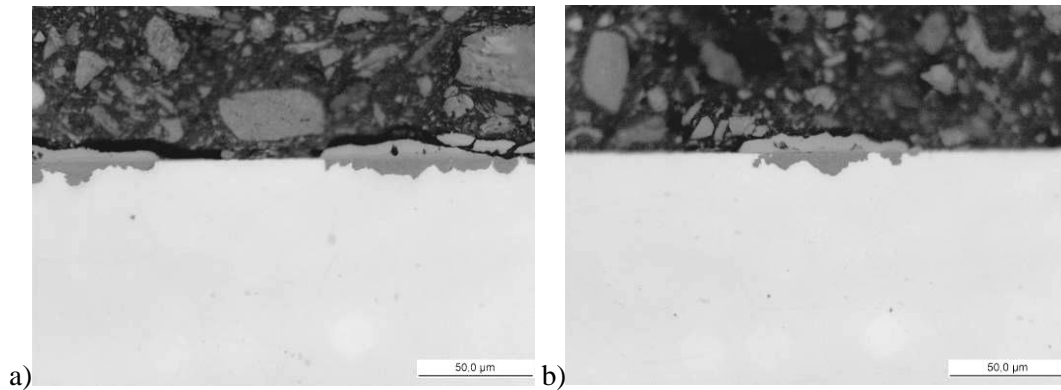


Figure 9. Oxide layers on a) TP347HFG(CN) and b) 347HFG after 1000 h at 650°C in air combustion environment; note spallation of outer oxide scale of TP347HFG(CN)

On steel HR3C, some localised oxide nodules were observed after 1000 h exposure at 650°C, Fig. 10. The two-layer oxide had an iron-rich outer layer with small amounts of chromium, and an inner layer of mixed oxide of chromium, nickel and iron. On Sanicro 25 and Ni alloys A263 and A617, only very thin oxide films (<1 µm) were found, characterised by GDOES measurements (see Appendix 2).



*Figure 10. Oxide nodules on HR3C after 1000 h exposure at 650°C in a) air combustion and b) oxyfuel combustions environment*

### 3.2 Exposure tests under CaCO<sub>3</sub>-CaSO<sub>4</sub> deposit at 650°C

The effect of synthetic CaCO<sub>3</sub>-CaSO<sub>4</sub> salt mixture on selected materials (X20, TP347HFG, HR3C, Sanicro 25, A263 and A617) under simulated oxyfuel atmosphere was studied at 650°C. Fig. 11 summarises the resulting oxide scale thickness measured with optical microscope, comparing the results from tests without deposit (gas exposure only) and with (under) deposit. Under gas exposure only, X20 and TP347HFG were oxidised already after 500 h. After 1000 h of exposure, some localised oxide nodules were also observed on HR3C but almost negligible oxidation occurred on Sanicro 25 and A263. No carburisation of metal was observed in tests without deposit.

Oxidation of all test materials was found to occur under deposit. The oxide scale on X20 and TP347HFG was continuous, and when comparing the oxide scale within the same specimen, the oxide formed under deposit (lower part of the specimen) was of similar composition but somewhat thicker and coarser than under gas atmosphere (upper part of the specimen), Fig. 12. Fig. 13 shows EDS mapping of oxide formed on X20, with a Fe-rich and Cr-depleted outer layer of the oxide. The deposit was also associated with accelerated oxidation of austenitic steels HR3C and Sanicro 25, and Ni-based superalloys, with oxide nodules found on the surfaces, Fig. 14. In addition to oxidation, carburisation of X20 and TP347HFG was observed, Fig. 15. Table 3 and Fig. 16 present the carbon content of TP347HFG surface at different depths, determined with optical emission spectrometry (Leco TC-136). The depth of carburisation on TP347HFG after 1000 h was 200-250 µm.

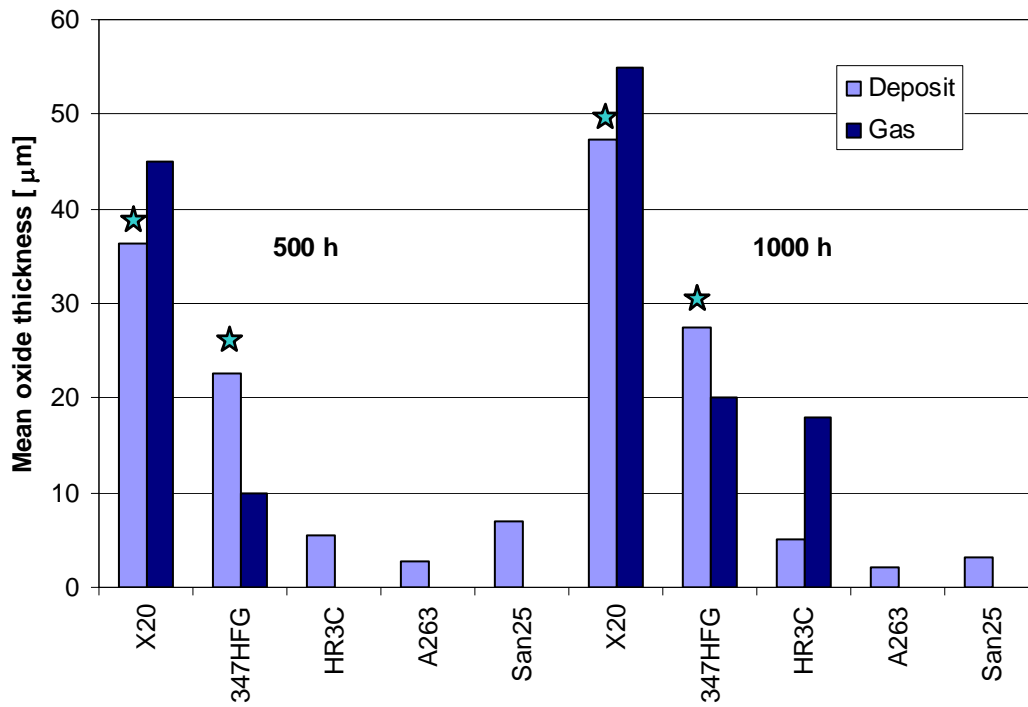


Figure 11. Observed oxide thickness on materials exposed to simulated oxyfuel conditions at 650°C with and without  $\text{CaCO}_3\text{-CaSO}_4$  deposit. For HR3C, Sanicro 25 and A263, oxide thickness corresponds to the mean nodule thickness. ★ carburisation of metal observed

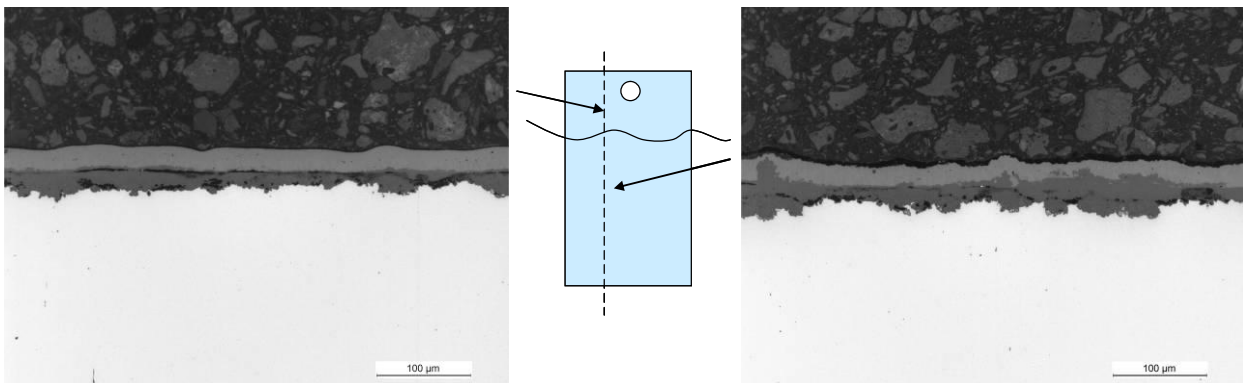
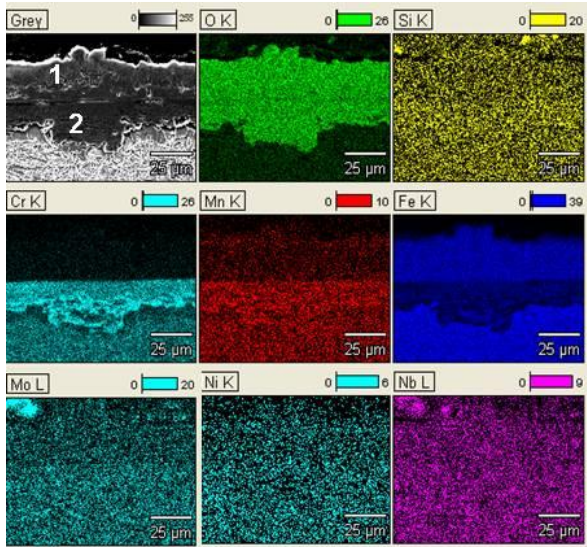


Figure 12. Oxide scale morphology on X20 after 1000 h with  $\text{CaCO}_3\text{-CaSO}_4$  in oxyfuel conditions at 650°C, under gas phase (left) and under deposit (right). The schematic specimen between micrographs shows sectioning and positions for inspection.





Wt%	1	2
O	22.0	29.4
Fe	77.3	46.8
Cr	0.6	20.0
Ca	0.1	-
Mn		1.2
Mo		1.1
		Si, V, Ni

Figure 13. EDS mapping and point analyses of oxide formed on X20 under  $\text{CaCO}_3\text{-CaSO}_4$  deposit.

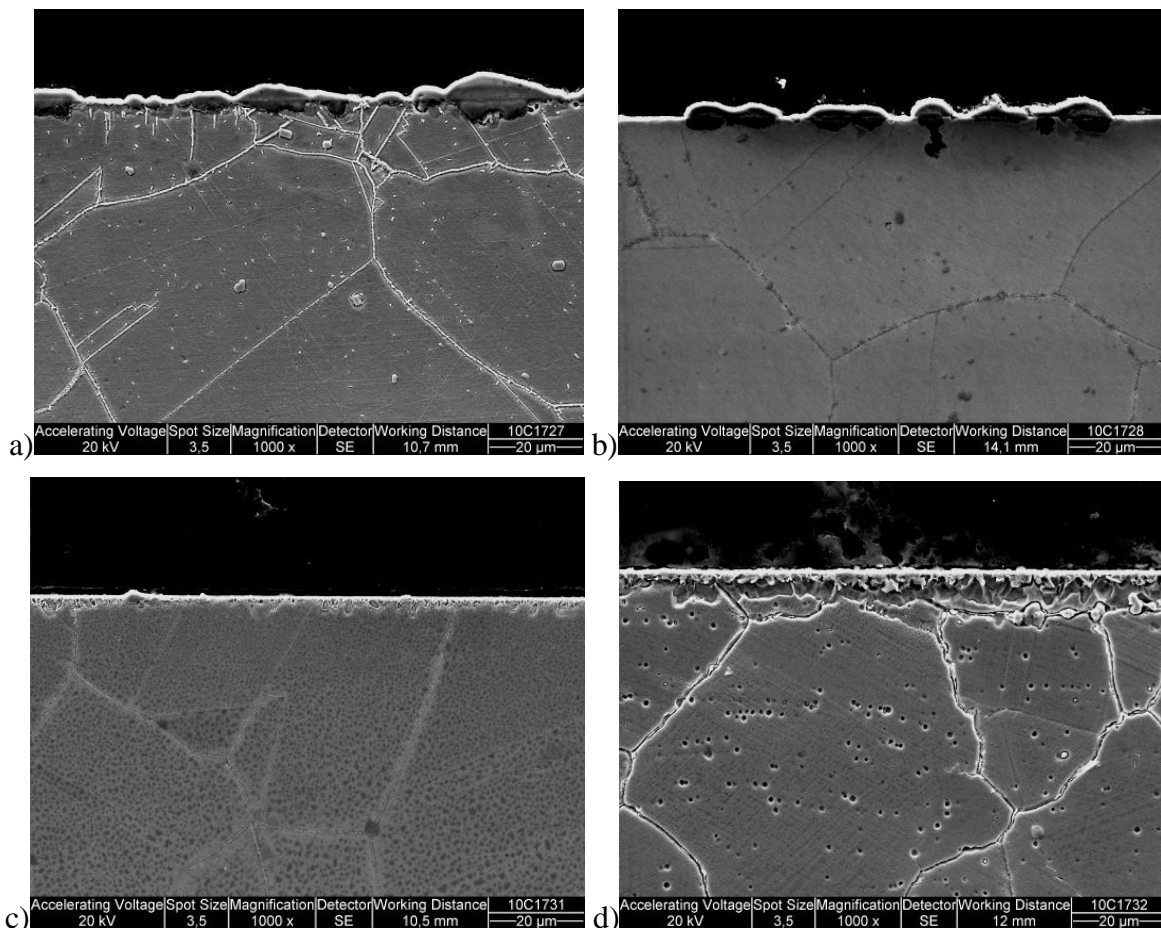


Figure 14. SEM micrographs of cross-sections after exposure for 1000 h at 650°C with  $\text{CaCO}_3\text{-CaSO}_4$  deposit in oxyfuel conditions: a) HR3C, b) Sanicro 25, c) A263 and d) A617

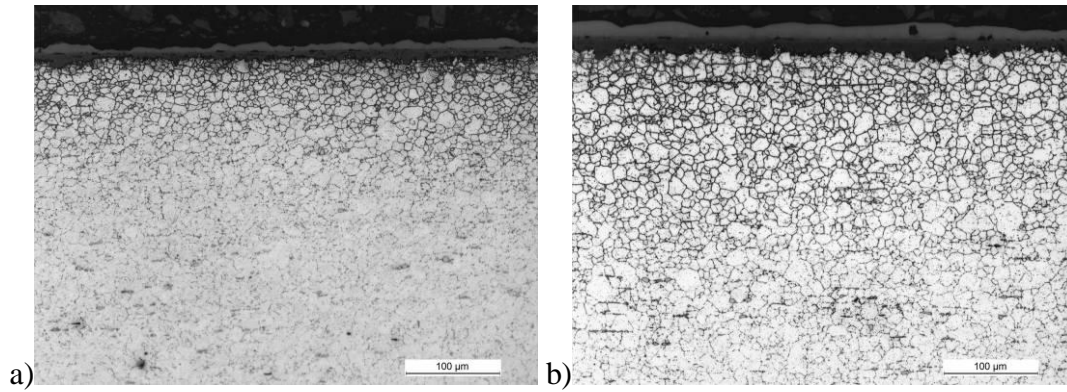


Figure 15. Carburisation of TP347HFG after a) 500 h and b) 1000 h under  $\text{CaCO}_3\text{-CaSO}_4$  deposit with simulated oxyfuel conditions at  $650^\circ\text{C}$ .

Table 4. Chemical composition as a function of depth of TP347HFG exposed to  $\text{CaCO}_3\text{-CaSO}_4$  under simulated oxyfuel conditions at  $650^\circ\text{C}$ ; note elevated C content near surface .

Composition	Fe	C	Cr	Ni	Mo	Other
as-received	bal	0.07	18.3	11.7	0.23	1.64 Mn, 0.92 Nb, 0.33 Cu, 0.02 Al
<b>After exposure</b>						
0.04 mm from surface	bal	0.2	18.4	11.5	0.24	1.66 Mn, 0.85 Nb, 0.36 Cu, 0.01 Al
0.06 mm from surface	bal	0.14	18.4	11.4	0.24	1.65 Mn, 0.86 Nb, 0.36 Cu, 0.014 Al
0.8 mm from surface	bal	0.07	18.4	11.6	0.24	1.67 Mn, 0.87 Nb, 0.36 Cu, 0.013 Al

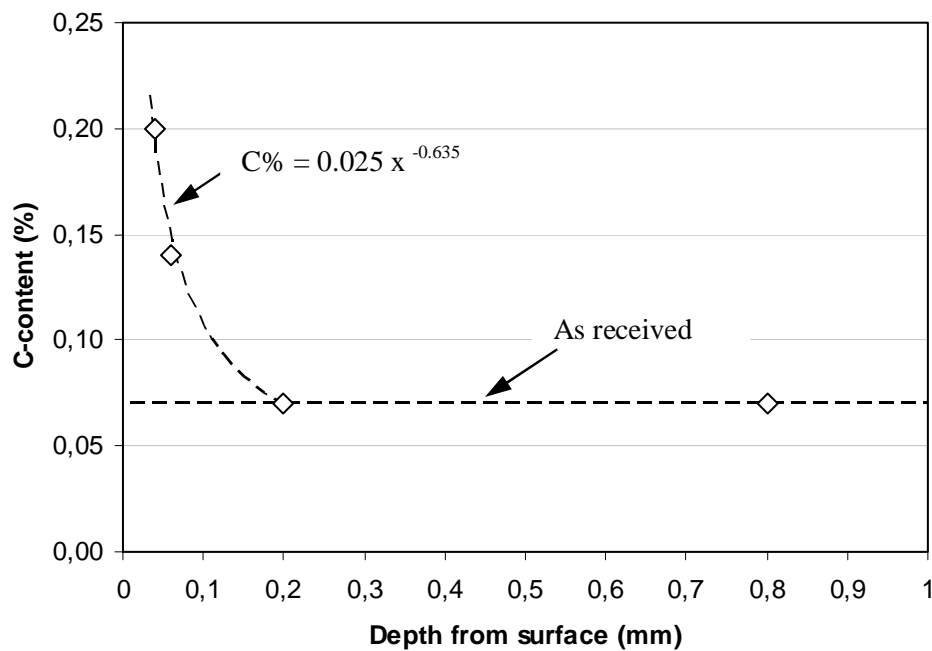


Figure 16. Carbon content on TP347HFG under deposit after exposure to simulated oxyfuel conditions for 1000 h at  $650^\circ\text{C}$  (from Table 3 and metallography, with a fitted profile)

## 4 Discussion and conclusions

The results imply that without deposit, the oxidation rate under simulated air firing conditions is higher than under simulated oxyfuel conditions. An exception to this is X20, for which the oxidation rates were high in all cases both at 600°C and 650°C, and for which the difference was not really significant (Table 2 and Fig 4). In this respect, contradictory results have been reported in the literature. For example, Hünert et al. [8] have shown oxidation rates of X20 that were lower in air firing than in oxyfuel firing conditions, while Covino et al. [4] have presented results where the opposite was observed.

The results from 1000 h exposure tests suggest that the scale structure formed on X20 is changing significantly when temperature increases from 600 to 650°C. The oxide scale formed at 650°C both in air firing and oxyfuel conditions has a porous inner layer, and such an oxide is not expected to be protective against aggressive environments. Also from conventional design point of view, the applied test temperatures span a range that is crossing the usual upper design limit for the steel grade X20CrMoV11-1 (see e.g. EN 10216-2).

In case of TP347HFG, the observed oxidation rate at 600°C was variable and showed apparent changing of order between air-firing and oxyfuel firing conditions (Fig 4). At 650°C the oxidation rate was more consistent for both batches of TP347HFG and for both air-fired and oxyfuel-fired conditions (Table 2 and Fig 4). The observed levels and scatter of oxide thickness suggest that at 600°C, the oxidation rate of TP347HFG is close to the borderline of protective behaviour under the studied gaseous atmospheres, so that small local differences in e.g. the state of specimen surfaces may result in significant differences in the oxidation rates. In contrast, at 650°C the oxides grow clearly faster and do not remain protective under either type of gaseous environments (air or oxyfuel). In all cases the oxide on TP347HFG had a two-layer structure and started by nodule formation at weak points such as grain boundaries. This would continue until a continuous oxide is covering the surfaces.

Although the oxidation rate for the tested alloys at 650°C was mostly higher under air-fired than oxyfuel testing conditions without deposits, added impurities like SO<sub>2</sub> and HCl or longer exposure times may change the situation.

There was also a difference in the observed oxidation resistance of TP347HFG from two different suppliers. Weaker oxide adherence resulted in spallation in case of TP347HFG(CN) that showed lower hardness (168 HV5) than TP347HFG (215 HV5). Higher hardness probably indicates higher degree of cold working of TP347HFG, and therefore potentially higher diffusion rate and availability of chromium at the metal surface to improve oxidation resistance.

The oxidation of HR3C under both atmospheres without deposit was relatively slow at 600°C but significantly faster at 650°C, with oxide nodules forming on the exposed surfaces (Fig 10). Other highly alloyed materials (Sanicro 25 and Ni alloys A263 and A617) showed almost negligible oxidation, with only a thin oxide film (< 1 µm) forming on the surfaces. No internal carburisation of any alloy was observed after exposure to gaseous environments without deposit. However, some carbon enrichment was indicated inside the oxide layer after 1000 h exposure under oxyfuel conditions at 650°C.



Oxidation of all test materials was found to occur under deposit. In particular, exposure with the carbonate deposit resulted in corrosion and carburisation of metal with formation of grain boundary carbides in X20 and TP347HFG steels under the simulated oxyfuel atmosphere of 60%CO<sub>2</sub>-30%H<sub>2</sub>O-4%O<sub>2</sub>-Ar. In this case, carburisation occurred both in the gaseous environment (in the part of specimen above the deposit) and under the deposit. The results of Abo Akademi University (Fig 17) indicate that CaCO<sub>3</sub> in the deposit can change the surface conditions, allowing carbon to penetrate into alloy. No carburisation was observed with CaSO<sub>4</sub> deposit only, but CaCO<sub>3</sub>-CaSO<sub>4</sub> deposit already changed the situation after 168 h of exposure. Some oxide nodule formation was also observed with higher alloyed materials, but no carburisation. The results suggest that the critical limits of Cr and Ni content for carburisation are around 20% under the applied gas and deposit environments. The limits may be affected by the Cr/Ni ratio, extended time of exposure, and changes in the chemical and thermodynamical equilibria of the surfaces due to gradual modification in alloys, its oxides and deposits.

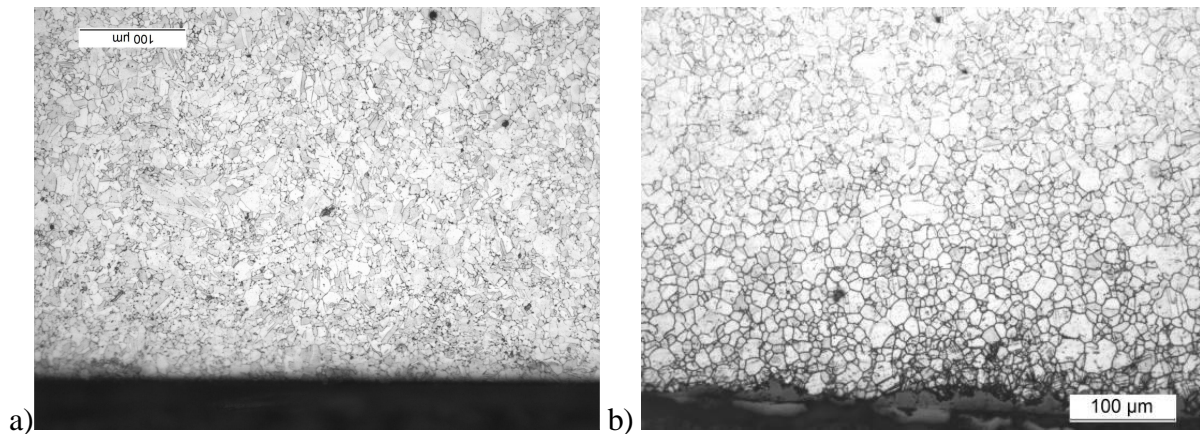
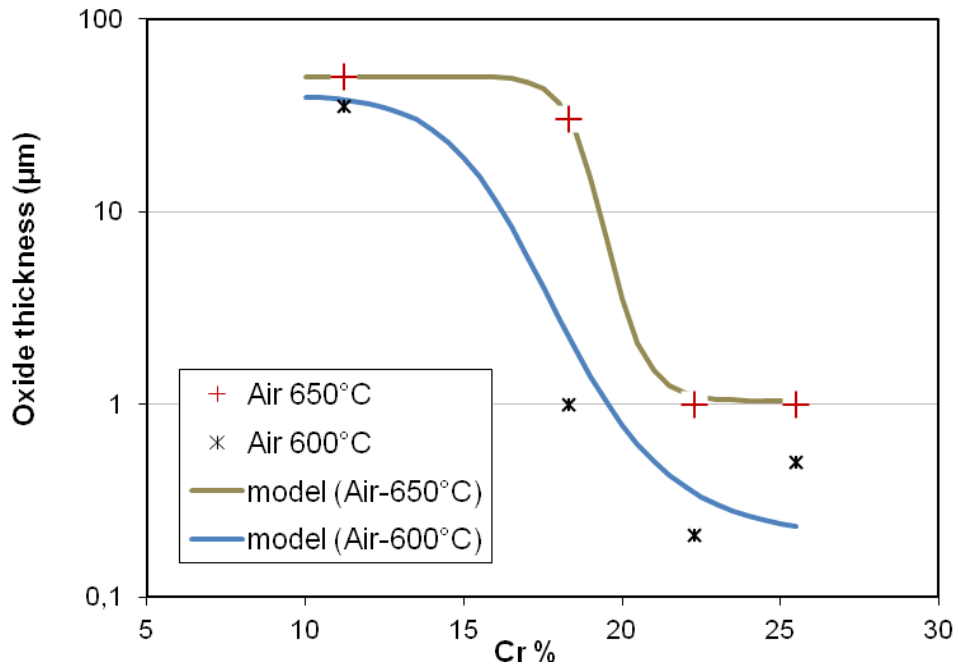


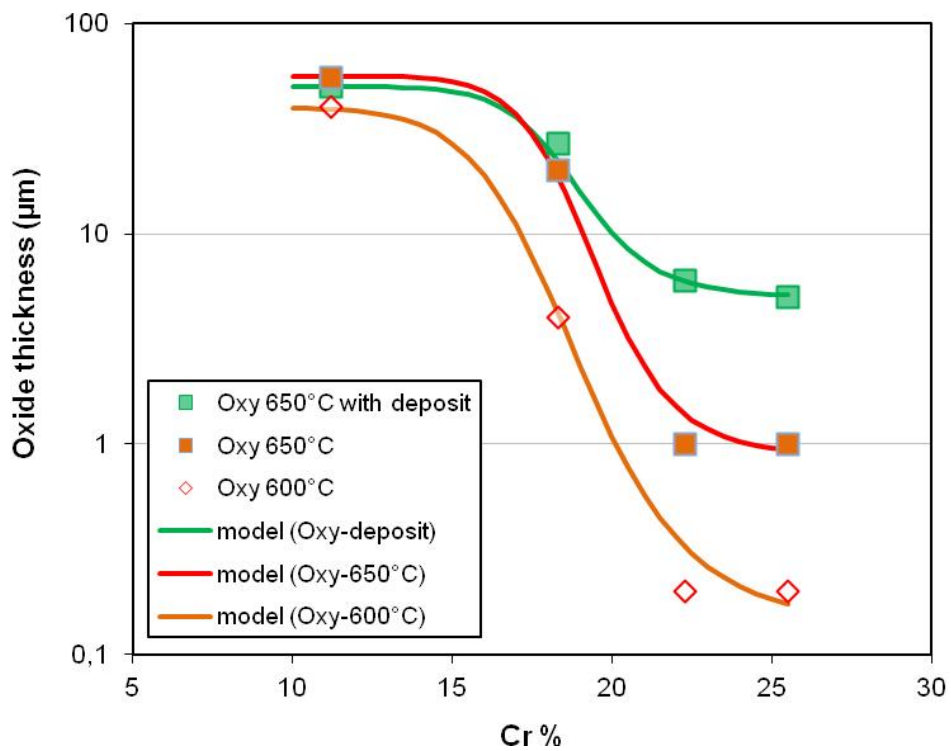
Figure 17. Micrographs of TP347HFG exposed at 650°C to a) CaSO<sub>4</sub> (no carburisation) and a) CaCO<sub>3</sub>-CaSO<sub>4</sub> deposit (with carburisation).

The results in terms of observed levels of oxide thickness are summarized in Table 4. The trend of oxidation rate of tested alloys as a function of Cr content is shown in Fig 18. In general, X20CrMoV11-1 at 600 and 650°C, and TP347HFG at 650°C do not appear to provide a well protective oxide in simulated air-fired or oxyfuel fired environments. In many cases somewhat faster oxidation appears to take place under a CaCO<sub>3</sub>-containing deposit than without the deposit, particularly at 650°C. This also applies to Sanicro 25 and to the tested Ni-alloys A263 and A617 that otherwise showed only thin surface oxides up to 1000 h of exposure under both air-fired and oxyfuel conditions. HR3C performed also reasonably well but did show a non-protective top oxide under simulated oxyfuel conditions without deposit at 650°C already after 500 h of exposure.

Non-protective oxide is generally indicated by a Fe-rich top layer oxide (see GDOES results in Appendix 2) which - unless it has spalled off - is usually clearly thicker than a protective oxide. It is notable that also carburisation of the metal surface up to a depth of about 200-250 μm was observed under the CaCO<sub>3</sub>-containing deposit on X20CrMoV11-1 and TP347HFG under simulated oxyfuel conditions, but not on other tested alloys or under the applied gaseous environment only (without deposit). In general, the thickness of a protective oxide layer was less than 6-10 μm in the test periods of the present work, i.e. up to 1000 h.



a)



b)

Figure 18. The oxidation rate of tested materials as function of Cr content in simulated a) air-fired and b) oxy-fired coal combustion conditions.

It is also to be noted all testing above was limited to untreated parent materials machined to the specified specimen geometry. Therefore, understanding the additional impact of e.g. welding or other additional processing related to fabrication may justify further work.

*Table 4. Summary of the observed oxide thickness on the tested materials after 1000 h of exposure, from direct and other (e.g. weight change) measurements*

Material	Environment	Oxide 600°C	Oxide 650°C	Notes
X20CrMoV11-1	Air firing, gas only Oxyfuel, gas only with deposit	~ 35 µm ~ 40 µm -	~ 50 µm ~ 55 µm ~ 50 µm *	Non-protective Fe-rich oxide on top surface
TP347HFG	Air firing, gas only Oxyfuel, gas only with deposit	< 1 µm 0.1-4 µm -	~ 30 µm ~ 20 µm ~ 27 µm *	Cr-rich oxide on top surface at 600°C, varies at 650°C
HR3C	Air firing, gas only Oxyfuel, gas only with deposit	0.2-0.5 µm 0.1-0.2 µm -	~ 0.5-1 µm ~ 1 µm ~ 5 µm	Cr-rich oxide on top surface at 600°C; Cr- or Fe-rich at 650°C
Sanicro 25	Air firing, gas only Oxyfuel, gas only with deposit	0.1-0.2 µm ~ 0.2 µm -	0.4 - 1 µm 0.5 - 1 µm ~ 2 - 6 µm	Cr-rich oxide on top surface
A263	Air firing, gas only Oxyfuel, gas only with deposit	< 0.2 µm < 0.2 µm -	~ 0.5 µm ~ 0.5 µm ~ 2 µm	Cr-rich oxide on top surface
A617	Air firing, gas only Oxyfuel, gas only with deposit	< 0.2 µm < 0.2 µm -	~ 0.5 µm ~ 0.6 µm -	Cr-rich oxide on top surface

\* with observed carburisation in the metal

## 5 Summary

Four boiler tube steels (X20CrMoV11-1, TP347HFG (from two sources), HR3C and Sanicro 25) and two Ni-based alloys (A263 and A617) have been subjected to oxidation/corrosion testing 600 and 650°C under simulated air-fired and oxyfuel fired atmospheres with and without CaCO<sub>3</sub>-CaSO<sub>4</sub> deposit.

Steel X20CrMoV11-1 at 600 and 650°C, and TP347HFG at 650°C did not show a well protective oxide after 1000 h exposure to simulated air-fired or oxyfuel fired environments. When a protective oxide was formed under a gaseous atmosphere, somewhat faster oxidation was observed under the deposit than without it, particularly at 650°C. This was also the case for Sanicro 25, A263 and A617 that otherwise only showed thin ( $\leq 1$  µm) surface oxides (mostly as nodules) up to 1000 h of exposure under both air-fired and oxyfuel conditions.

The tested materials retained an oxide without notable spalling, with the exception of TP347HFG(CN) steel that suffered spallation of the outer oxide layer after 1000 h exposure at 650°C. Without deposits the simulated oxyfuel atmosphere with high CO<sub>2</sub> and moisture



content did not appear to result in more severe oxidation than with simulated air firing conditions. No carburisation was observed after exposure to gaseous environments only, except for some carbon enrichment at oxide-surface interface. However, carburisation of X20CrMoV11-1 and TP347HFG up to a depth of about 0.25 mm was found after 1000 h exposure to the simulated oxyfuel environment with CaCO<sub>3</sub>-CaSO<sub>4</sub> deposit.

In real oxyfuel combustion the flue gas recirculation will also increase the concentration of corrosive impurities such as sulphur and chlorides. Corrosion, microstructural and other changes, like carburisation, may reduce mechanical performance such as creep and/or fatigue strength and ductility, and thus the expected component life. In addition, long term operation and additional impact from local effects such as welds other other features from fabrication, assembly or repairs could influence the phenomena and conclusions described above, possibly justifying further work for clarification.

## 6 Acknowledgements

The authors thank the skilful assistance of T. Kinnunen, J. Veivo, T. Lehtikuusi, M. Mattila, K. Nöjd, P. Varis and S. Holmström in the experimental work.

## References

1. Energy Visions 2050, WS Bookwell oy, 2009 Porvoo, 380 p. ISBN 978-951-37-5595-9
2. Järnäs, A., Svensson, J.-E., Johansson, L.-G. Inhibitive effect of traces of SO<sub>2</sub> on the oxidation of iron. *Oxidation of Metals* Vol. 60 (2003). pp. 427-445
3. Tuurna, S., Środa, S., Heikinheimo, L. Corrosion Kinetics and Mechanism of Boiler Steels under Combustion Conditions. *Baltica VI: Life Management and Maintenance for Power Plants*, Vol. 1, Helsinki-Stockholm-Helsinki, 8-10 June, 2004.
4. B. Covino, S. Matthes, S. Bullard, Effect of Oxyfuel Combustion on Superheater Corrosion, NACE2008, Paper 8456
5. Natesan, K. & Rink, D. L., Corrosion performance of structural alloys for oxy-fuel combustion systems, 21st Fossil Energy Materials Conference, Knoxville, TN (2007).
6. Fry, A., Adams, B., Davis, K., Swensen, D., Munson, S. Fire-side corrosion rates of heat transfer surface materials for air- and oxy-coal combustion. IEAGHG Special Worksop on SO<sub>2</sub>/SO<sub>3</sub>/Hg/Corrosion Issue under Oxyfuel Combustion Conditions, January 2011, London
7. Kiga, T. Experimental study results on corrosion issues in oxyfuel combustion process. IEAGHG Special Worksop on SO<sub>2</sub>/SO<sub>3</sub>/Hg/Corrosion Issue under Oxyfuel Combustion Conditions, January 2011, London
8. D. Hünert, W. Schulz and A. Kranzmann. Corrosion of steels in H<sub>2</sub>O-CO<sub>2</sub> atmospheres at temperatures between 500°C and 700°C, ICPWS XV Berlin, September 8–11, 2008
9. J. Piron Abellan, T. Olszewski, H.J. Penkalla, G.H. Meier, L. Singheiser, W.J. Quadackers, Scale formation mechanisms of martensitic steels in high CO<sub>2</sub>/H<sub>2</sub>O-containing gases simulating oxyfuel environments. *Materials at high temperatures* (26) 2009, pp. 63-72
10. L. Fryda, C. Sobrino, M. Cieplik and W.L. van de Kamp. Study on ash deposition under oxyfuel combustion of coal/biomass blends. *Fuel* (2010), Vol. 89, pp. 1889-1902
11. Stein-Brzozowska, G., Maier, J., Scheffnecht, G. Deposition behaviour and superheater corrosion under coal fired oxyfuel conditions. IEAGHG Special Worksop on

- SO<sub>2</sub>/SO<sub>3</sub>/Hg/ Corrosion Issue under Oxyfuel Combustion Conditions, January 2011, London
12. B.J.P. Buhre, L.K. Elliott, C.D. Sheng, R.P. Gupta and T.F. Wall. Oxy-fuel combustion technology for coal-fired power generation. *Progress in Energy and Combustion Science* (2005), Vol 31, Issue 4, Pp 283-307
  13. S.R.J. Saunders, M. Montero, F. Rizzo, The oxidation behaviour of metals and alloys at high temperatures in atmospheres containing water vapour: A review. *Progress in Materials Science* 53 (2008), pp. 775-837
  14. J. Ehlers, D.J. Young, E.J. Smaardijk, A.K. Tyagi, H.J. Penkalla, L. Singheiser and W.J. Quadackers. Enhanced oxidation of the 9%Cr steel P91 in water vapour containing environments. *Corrosion Science*, Vol 48, Issue 11 (2006), pp. 3428-3454
  15. Hünert, D., Kranzmann, A. Influence of pressure and chromium content on corrosion reactions at 600°C in a CO<sub>2</sub>-H<sub>2</sub>O atmosphere. NACE 2008, paper no. 8447
  16. Giggins, Pettit, Corrosion of metals and alloys in mixed gas environments at elevated temperature. *Oxidation of Metals* 14(5) 1980, pp. 363-413
  17. Meier, Coons, Perkins. Corrosion of iron-, nickel- and cobalt-base alloys in atmospheres containing carbon and oxygen. *Oxidation of Metals* 17(3/4) 1982, 235-262
  18. Grabke, H.-J., Ohla, K., Peters, J, Wolf, I., *Materials and Corrosion* 34 (1983), pp. 495-500
  19. D. Hünert and A. Kranzmann. Impact of oxyfuel atmospheres H<sub>2</sub>O/CO<sub>2</sub>/O<sub>2</sub> and H<sub>2</sub>O/CO<sub>2</sub> on the oxidation of ferritic-martensitic and austenitic steels. *Corrosion Science* 53 (2011), pp. 2306-2317
  20. Mäkipää, M. Corrosion mechanisms and thermodynamics in atmospheres with CO<sub>2</sub>, VTT-R-04861-11 (2011)
  21. Tuurna, S. High performance materials and corrosion control for efficient and low emission biomass and waste combustion – Final report. VTT-R-02825-11 (2011)

## Results of analyses for exposed samples

Sample	Atmosp.	Temp [°C]	Salt	Steel	Thickness			Time [h]	$\Delta m$ [mg/cm <sup>2</sup> ]
					Mean	St. dev	Max		
3.9	AIR-FIRING	600		X20	35	4.2	40	1000	4.676
3.10	AIR-FIRING	600		X20				1000	5.738
4.9	AIR-FIRING	600		347HFG(CN)				1000	0.038
4.10	AIR-FIRING	600		347HFG(CN)	0			1000	0.042
5.9	AIR-FIRING	600		347HFG	0.3			1000	0.030
5.10	AIR-FIRING	600		347HFG				1000	0.027
6.9	AIR-FIRING	600		HR3C	0.3			1000	0.043
6.10	AIR-FIRING	600		HR3C				1000	0.019
9.9	AIR-FIRING	600		Sanicro 25	0.2			1000	0.004
9.10	AIR-FIRING	600		Sanicro 25				1000	0.030
3.11	OXYFUEL	600		X20				1000	1.048
3.12	OXYFUEL	600		X20	42	6.4	53	1000	4.422
4.11	OXYFUEL	600		347HFG(CN)				1000	-0.005
4.12	OXYFUEL	600		347HFG(CN)				1000	0.005
5.11	OXYFUEL	600		347HFG	0.3			1000	-0.017
5.12	OXYFUEL	600		347HFG				1000	0.351
6.11	OXYFUEL	600		HR3C	0.3			1000	-0.007
6.12	OXYFUEL	600		HR3C				1000	0.004
9.11	OXYFUEL	600		Sanicro 25	0.2			1000	-0.001
9.12	OXYFUEL	600		Sanicro 25				1000	-0.020
3.15	AIR-FIRING	650		X20			20	168	0.064
3.16	AIR-FIRING	650		X20	30.2	3.74	32.7	168	0.325
5.15	AIR-FIRING	650		347HFG			18	168	0.972
5.16	AIR-FIRING	650		347HFG			8	168	0.569
6.15	AIR-FIRING	650		HR3C				168	0.006
6.16	AIR-FIRING	650		HR3C				168	0.036
7.15	AIR-FIRING	650		A263(Nimonic)				168	0.012
7.16	AIR-FIRING	650		A263(Nimonic)				168	0.009
8.15	AIR-FIRING	650		A617 (Inconel)				168	-0.009
8.16	AIR-FIRING	650		A617 (Inconel)				168	0.005
9.15	AIR-FIRING	650		Sanicro 25				168	0.015
9.16	AIR-FIRING	650		Sanicro 25				168	0.004
3.7	AIR-FIRING	650		X20			35	500	0.036
3.8	AIR-FIRING	650		X20				500	0.045
5.7	AIR-FIRING	650		347HFG				500	2.730
5.8	AIR-FIRING	650		347HFG				500	0.074
6.7	AIR-FIRING	650		HR3C	0.4			500	0.323
6.8	AIR-FIRING	650		HR3C				500	0.021
7.7	AIR-FIRING	650		A263(Nimonic)				500	0.048
7.8	AIR-FIRING	650		A263(Nimonic)				500	0.033
8.7	AIR-FIRING	650		A617 (Inconel)	0.6			500	0.048
8.8	AIR-FIRING	650		A617 (Inconel)				500	0.053
9.7	AIR-FIRING	650		Sanicro 25	0.2			500	0.012
9.8	AIR-FIRING	650		Sanicro 25				500	0.028
3.3	AIR-FIRING	650		X20	52.1	7.3	59.9	1000	5.905
3.4	AIR-FIRING	650		X20				1000	4.349
4.3	AIR-FIRING	650		347HFG(CN)	spallation			1000	1.970
4.4	AIR-FIRING	650		347HFG(CN)				1000	1.135

5.2	AIR-FIRING	650		347HFG	30.7	10.1	48.1	1000	2.286
5.4	AIR-FIRING	650		347HFG				1000	2.453
6.3	AIR-FIRING	650		HR3C				1000	0.230
6.4	AIR-FIRING	650		HR3C				1000	0.160
7.3	AIR-FIRING	650		A263(Nimonic)				1000	0.054
7.4	AIR-FIRING	650		A263(Nimonic)				1000	0.075
8.3	AIR-FIRING	650		A617 (Inconel)				1000	-0.066
8.4	AIR-FIRING	650		A617 (Inconel)				1000	0.038
9.3	AIR-FIRING	650		Sanicro 25				1000	0.072
9.4	AIR-FIRING	650		Sanicro 25				1000	0.068
3.13	OXYFUEL	650		X20				168	0.744
3.14	OXYFUEL	650		X20	19.6	3.6	22.9	168	1.565
5.13	OXYFUEL	650		347HFG	18.5	3.4	20.6	168	0.052
5.14	OXYFUEL	650		347HFG	9.3	3.2	13	168	0.022
6.13	OXYFUEL	650		HR3C				168	0.002
6.14	OXYFUEL	650		HR3C				168	0.018
7.13	OXYFUEL	650		A263(Nimonic)				168	0.020
7.14	OXYFUEL	650		A263(Nimonic)				168	0.039
8.13	OXYFUEL	650		A617 (Inconel)				168	-0.002
8.14	OXYFUEL	650		A617 (Inconel)				168	0.002
9.13	OXYFUEL	650		Sanicro 25				168	0.014
9.14	OXYFUEL	650		Sanicro 25				168	0.016
3.5	OXYFUEL	650		X20	45.6	4.1	49	500	5.745
3.6	OXYFUEL	650		X20				500	5.727
5.5	OXYFUEL	650		347HFG			10	500	0.151
5.6	OXYFUEL	650		347HFG				500	2.023
6.5	OXYFUEL	650		HR3C	0.6			500	0.024
6.6	OXYFUEL	650		HR3C				500	0.177
7.5	OXYFUEL	650		A263(Nimonic)				500	0.023
7.6	OXYFUEL	650		A263(Nimonic)				500	0.008
8.5	OXYFUEL	650		A617 (Inconel)	0.4			500	-0.053
8.6	OXYFUEL	650		A617 (Inconel)				500	-0.048
9.5	OXYFUEL	650		Sanicro 25	0.6			500	0.040
9.6	OXYFUEL	650		Sanicro 25				500	0.007
3.1	OXYFUEL	650		X20	53.3	3.7	56.5	1000	8.228
3.2	OXYFUEL	650		X20				1000	5.141
4.1	OXYFUEL	650		347HFG(CN)	Some nodules , max 20 µm			1000	0.932
4.2	OXYFUEL	650		347HFG(CN)				1000	0.108
5.1	OXYFUEL	650		347HFG				1000	0.126
5.3	OXYFUEL	650		347HFG	16.1	4.8	19.3	1000	0.818
6.1	OXYFUEL	650		HR3C				1000	0.062
6.2	OXYFUEL	650		HR3C				1000	0.120
7.1	OXYFUEL	650		A263(Nimonic)				1000	0.051
7.2	OXYFUEL	650		A263(Nimonic)				1000	0.048
8.1	OXYFUEL	650		A617 (Inconel)				1000	-0.063
8.2	OXYFUEL	650		A617 (Inconel)				1000	-0.061
9.1	OXYFUEL	650		Sanicro 25				1000	-0.009
9.2	OXYFUEL	650		Sanicro 25				1000	-0.017
3.17	OXYFUEL	650	CaCO3- CaSO4	X20	36.3	5.5	43	500	
3.18	OXYFUEL	650	CaCO3- CaSO4	X20				500	
4.17	OXYFUEL	650	CaCO3- CaSO4	347HFG(CN)	30.7	12.1	42	500	

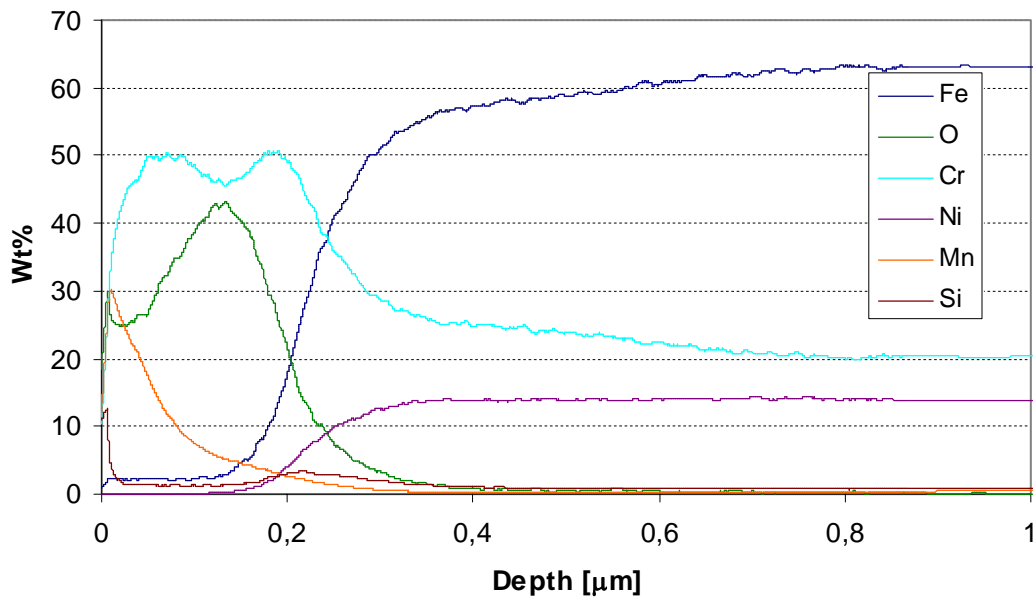
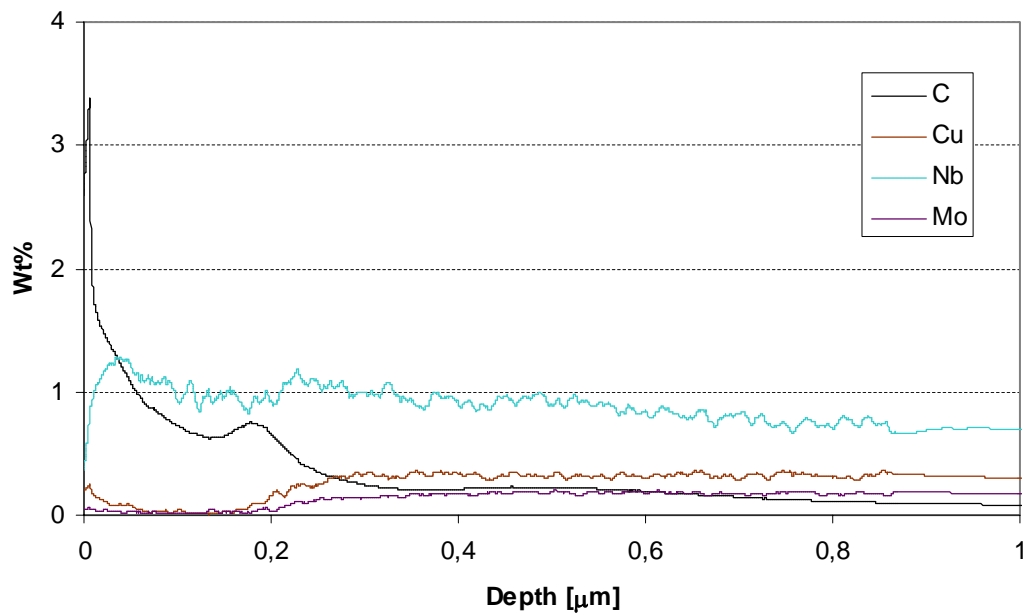
4.18	OXYFUEL	650	CaCO <sub>3</sub> - CaSO <sub>4</sub>	347HFG(CN)				500	
5.17	OXYFUEL	650	CaCO <sub>3</sub> - CaSO <sub>4</sub>	347HFG	22.7	7.5	30	500	
5.18	OXYFUEL	650	CaCO <sub>3</sub> - CaSO <sub>4</sub>	347HFG				500	
6.17	OXYFUEL	650	CaCO <sub>3</sub> - CaSO <sub>4</sub>	HR3C	5.5	2.1	7	500	
6.18	OXYFUEL	650	CaCO <sub>3</sub> - CaSO <sub>4</sub>	HR3C				500	
7.17	OXYFUEL	650	CaCO <sub>3</sub> - CaSO <sub>4</sub>	A263(Nimonic)	2.8	0.4	3	500	
7.18	OXYFUEL	650	CaCO <sub>3</sub> - CaSO <sub>4</sub>	A263(Nimonic)				500	
8.17	OXYFUEL	650	CaCO <sub>3</sub> - CaSO <sub>4</sub>	A617 (Inconel)			2.5	500	
8.18	OXYFUEL	650	CaCO <sub>3</sub> - CaSO <sub>4</sub>	A617 (Inconel)				500	
9.17	OXYFUEL	650	CaCO <sub>3</sub> - CaSO <sub>4</sub>	Sanicro 25			7	500	
9.18	OXYFUEL	650	CaCO <sub>3</sub> - CaSO <sub>4</sub>	Sanicro 25				500	
3.19	OXYFUEL	650	CaCO <sub>3</sub> - CaSO <sub>4</sub>	X20	47.4	14.7	69.3	1000	
5.19	OXYFUEL	650	CaCO <sub>3</sub> - CaSO <sub>4</sub>	347HFG	27.5	10.1	39.4	1000	
6.19	OXYFUEL	650	CaCO <sub>3</sub> - CaSO <sub>4</sub>	HR3C	5.1	1.1	6.4	1000	
7.19	OXYFUEL	650	CaCO <sub>3</sub> - CaSO <sub>4</sub>	A263(Nimonic)	2.2			1000	
8.19	OXYFUEL	650	CaCO <sub>3</sub> - CaSO <sub>4</sub>	A617 (Inconel)				1000	
9.19	OXYFUEL	650	CaCO <sub>3</sub> - CaSO <sub>4</sub>	Sanicro 25	3.2	0.3	3.5	1000	

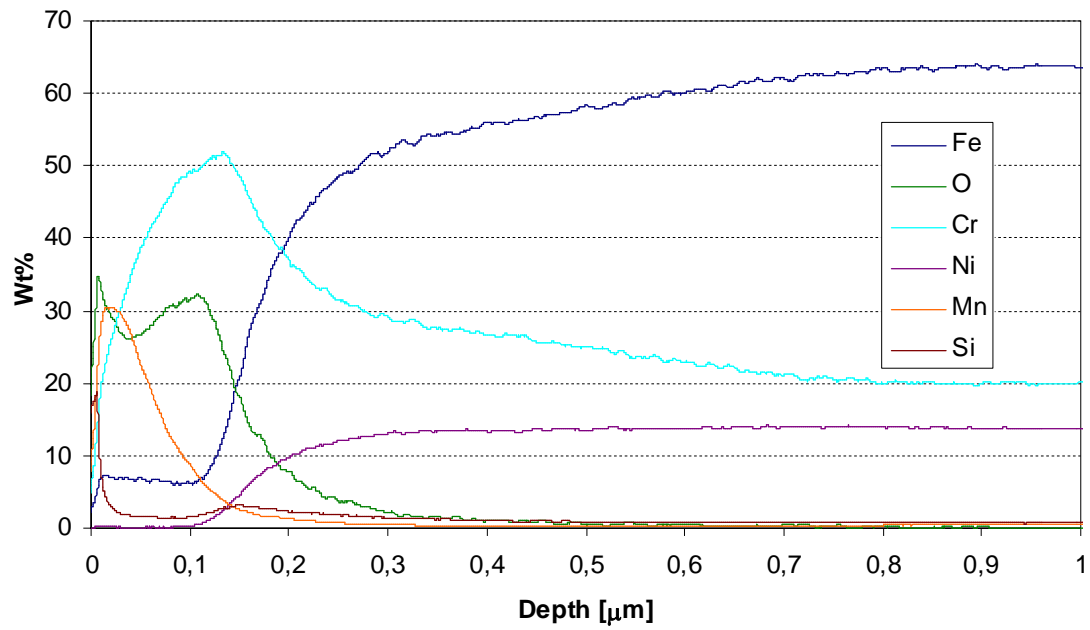
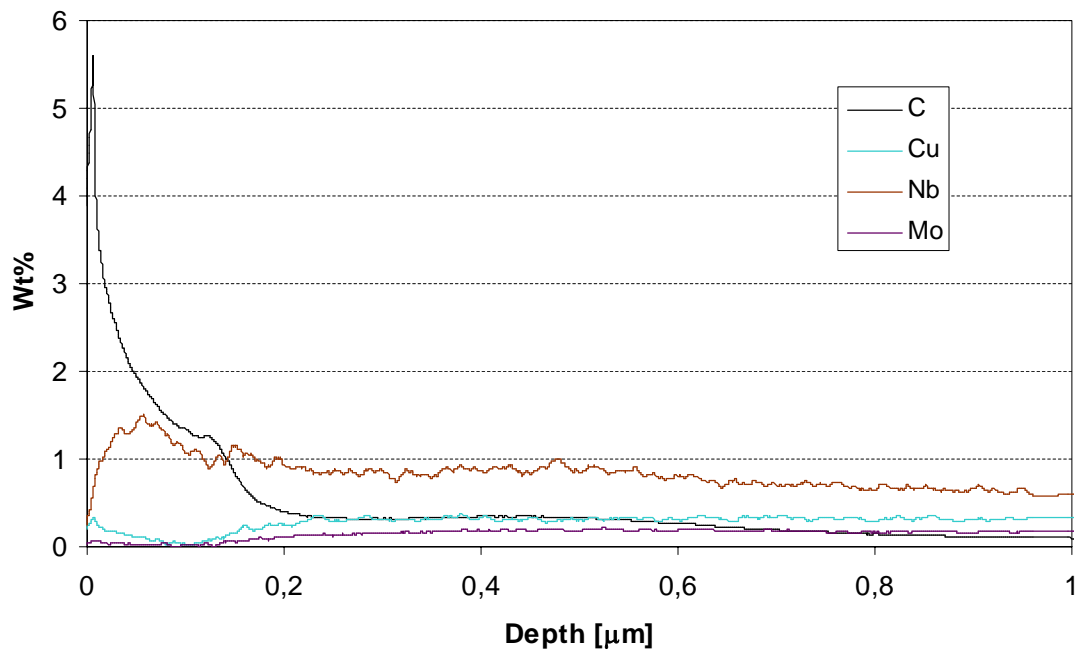
## GDOES analyses

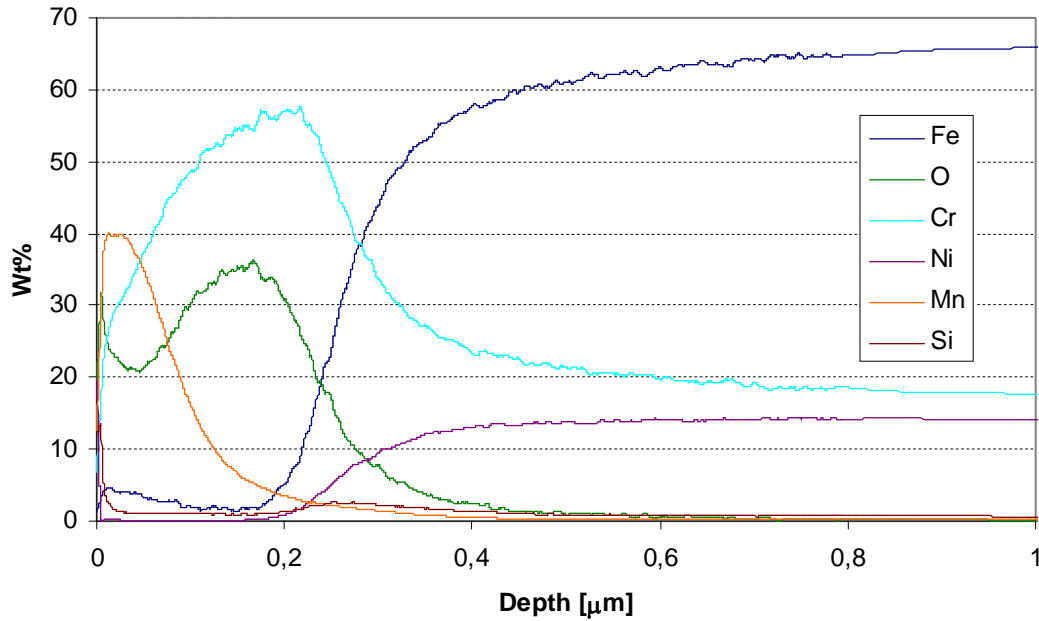
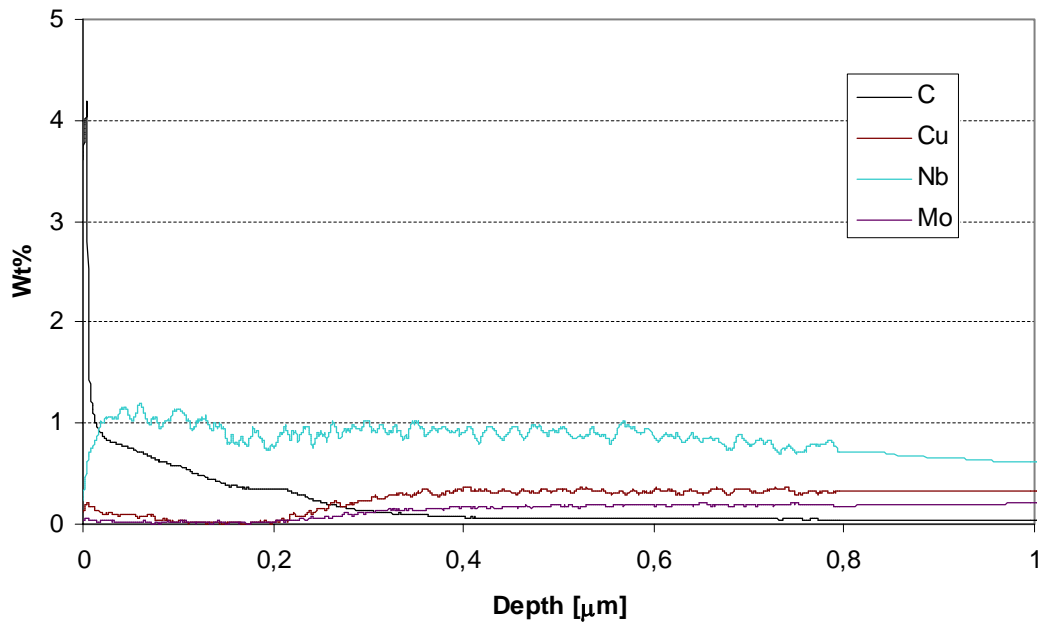
### *SPECIMENS FOR GDOES ANALYSIS*

Environment	Test n:o	Exposure T, °C	Duration, h	Material	Specimen
Oxyfuel	Hicor 3	600	1000	TP347HFG	5.11
				Sanicro 25	9.11
				HR3C	6.11
	Hicor 8	650	500	TP347HFG	5.6
				Sanicro 25	9.5
				HR3C	6.5
				A617	8.5
Air	Hicor 6	600	1000	TP347HFG	5.9
				Sanicro 25	9.9
				HR3C	6.9
	Hicor 11	650	500	TP347HFG	5.8
				Sanicro 25	9.7
				HR3C	6.7
				A617	8.7

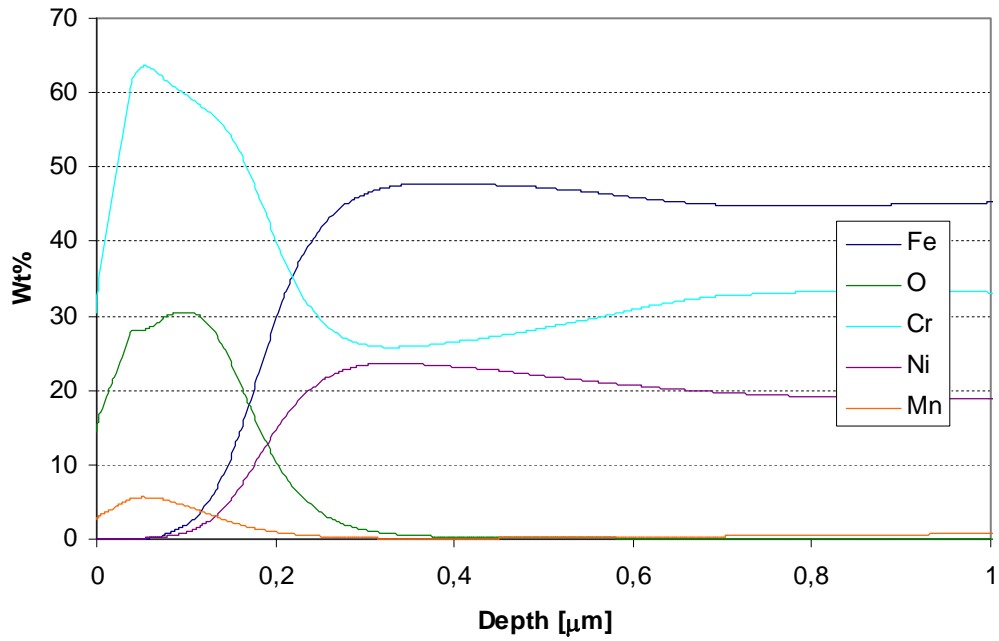
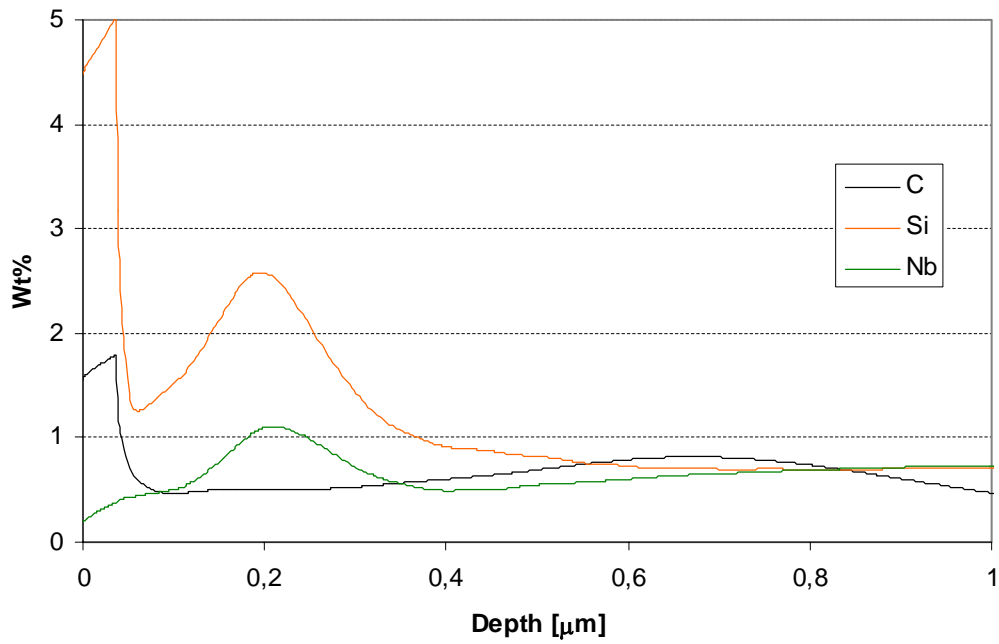


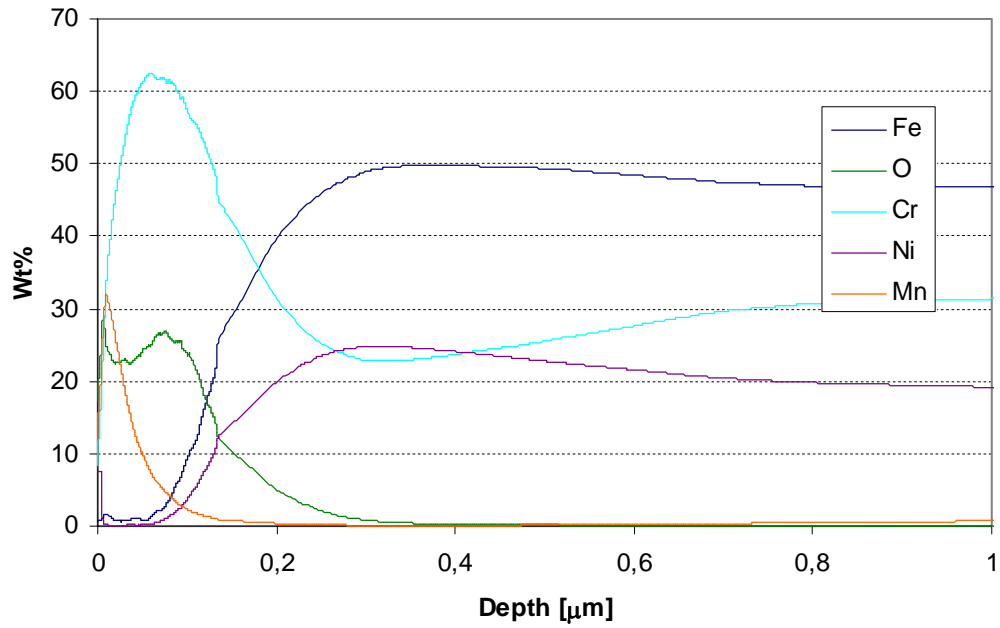
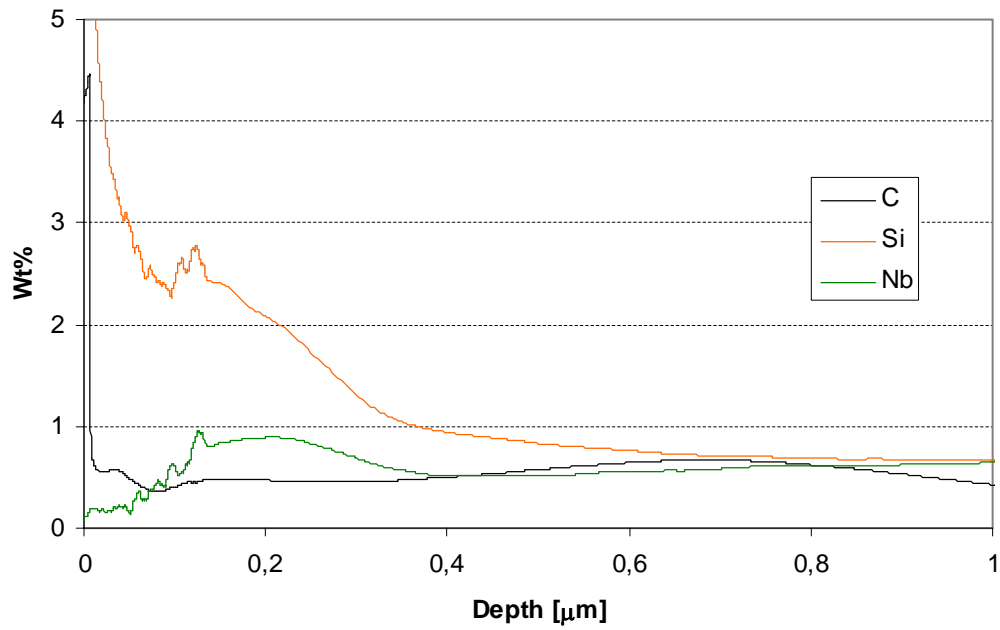
**TP347HFG, 600° - 1000h , air**

**TP347HFG, 600° - 1000h , air**


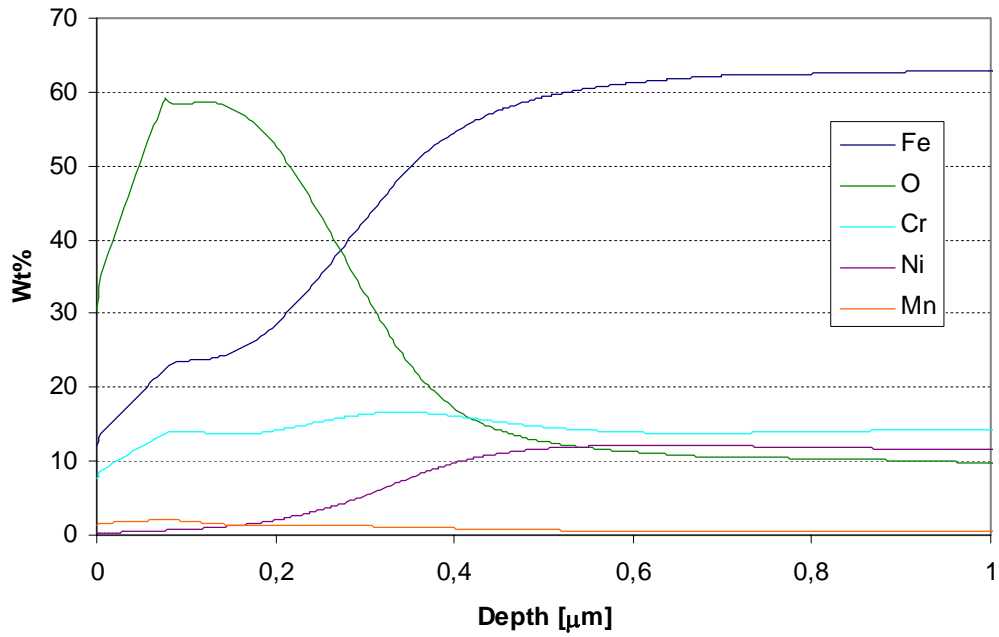
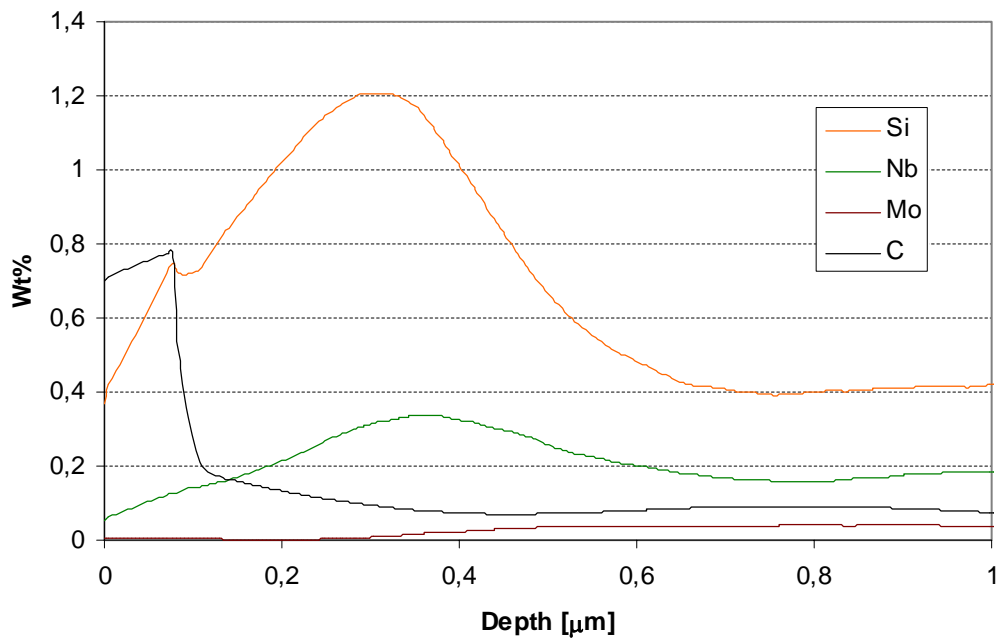
**TP347HFG 600°C - 1000 h, oxy**

**TP347HFG 600°C - 1000 h, oxy**


**TP347HFG, 650°C - 500 h, air**

**TP347HFG, 650°C - 500 h, air**


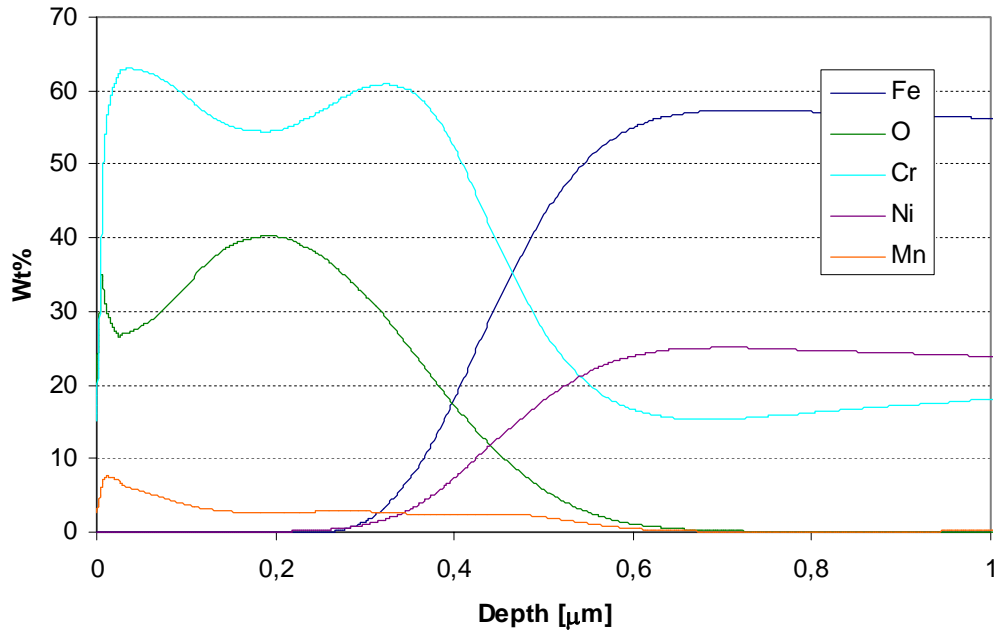
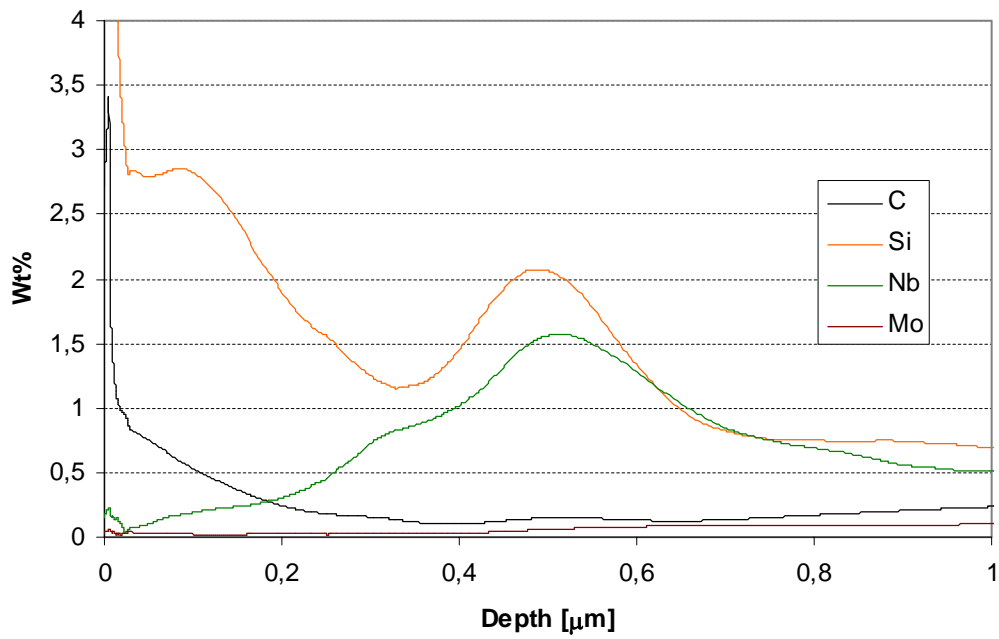
TP347HFG, 650°C, 500 h in oxy (sample 5.6) was not possible to measure. The surface roughness was too big (spallation of oxide,  $\Delta m$  with spalled oxides 2 mg/cm<sup>2</sup>)

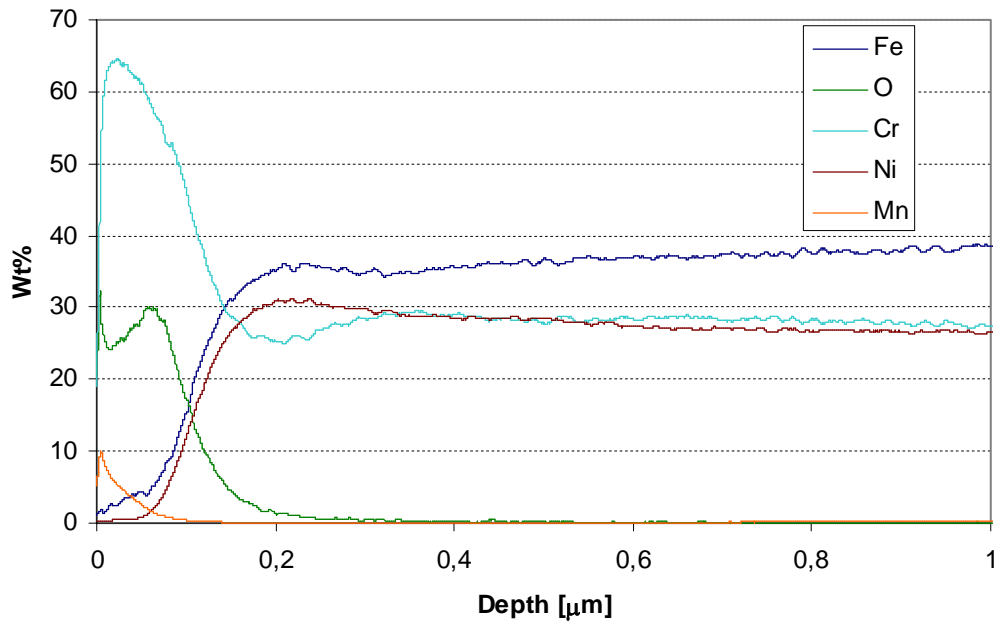
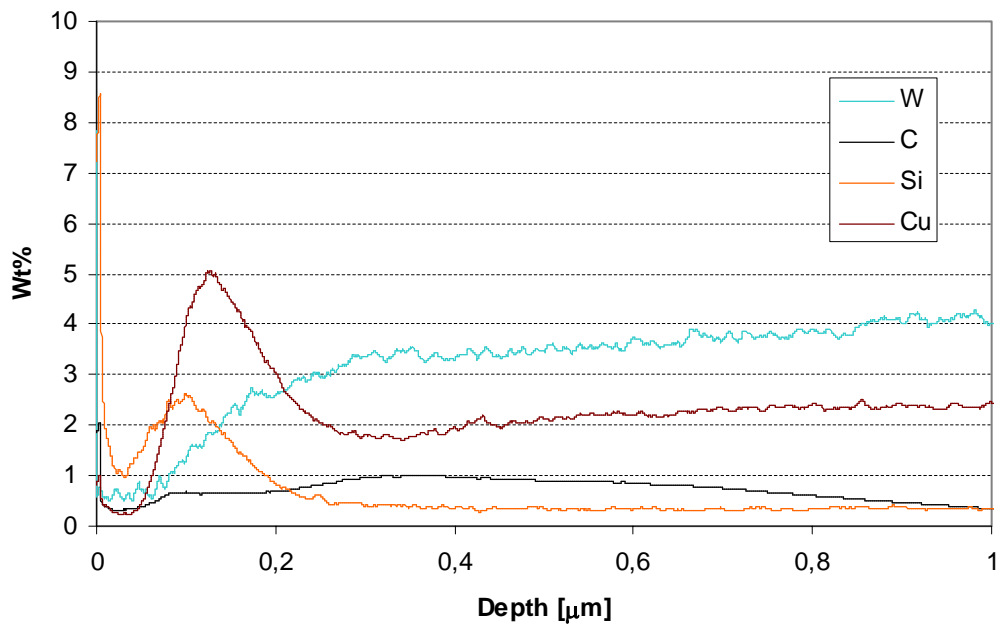
**HR3C, 600°C - 1000 h, air**

**HR3C, 600°C - 1000 h, air**


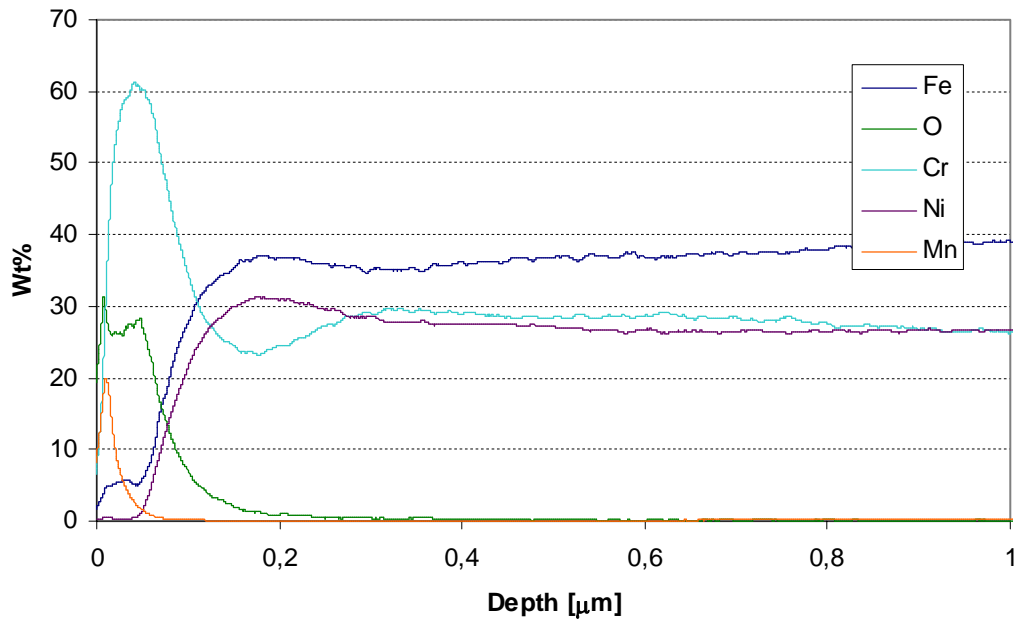
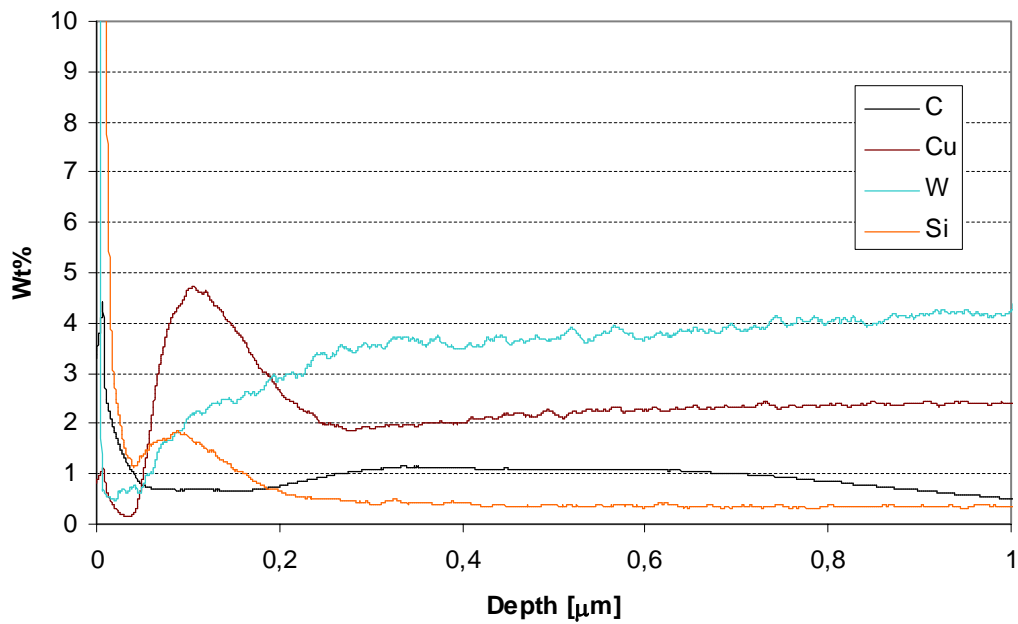
**HR3C, 600°C - 1000 h, oxy**

**HR3C, 600°C - 1000 h, oxy**


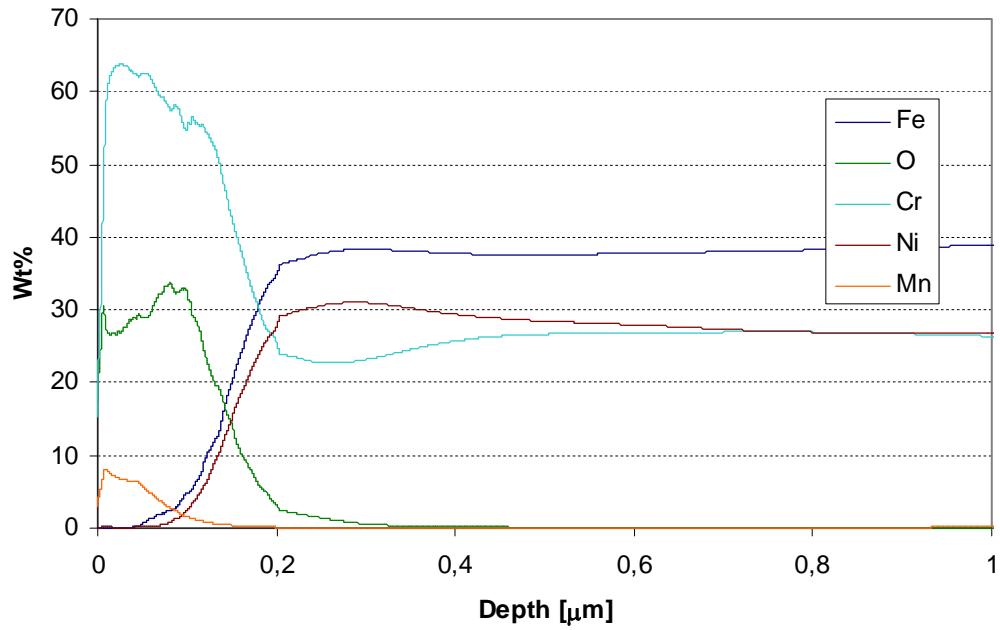
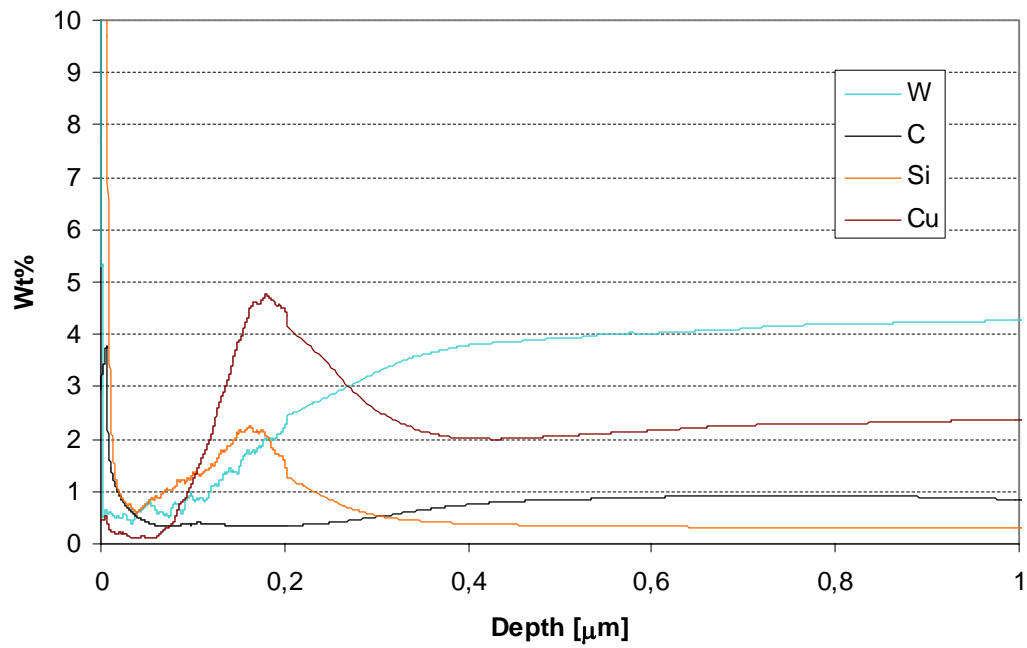
**HR3C, 650°C - 500 h, air**

**HR3C, 650°C - 500 h, air**




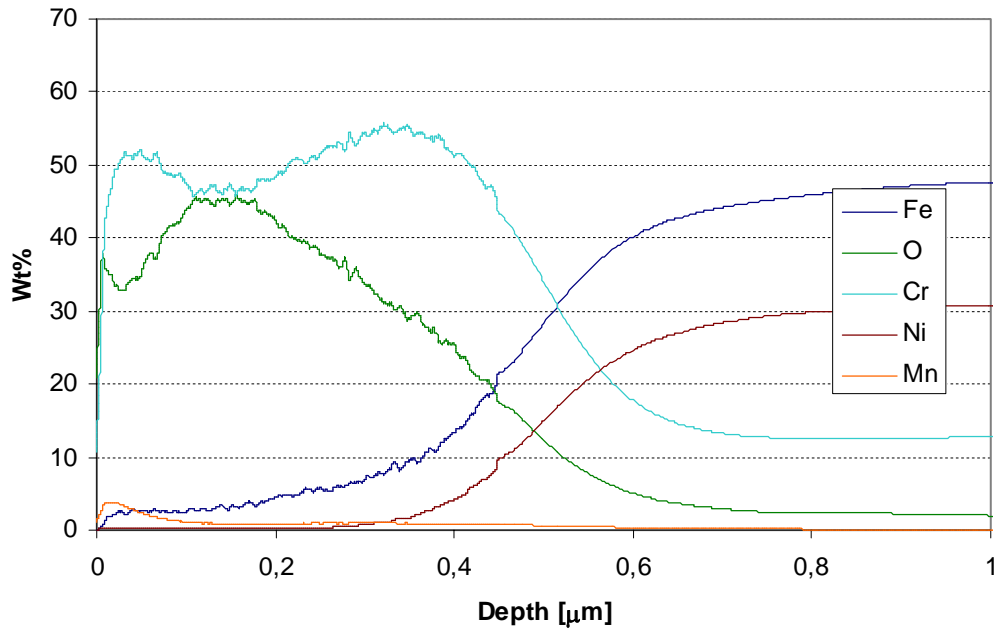
**HR3C, 650°C - 500 h, oxy**

**HR3C, 650°C - 500 h, oxy**


**Sanicro 25, 600°C- 1000 h, air**

**Sanicro 25, 600°C- 1000 h, air**


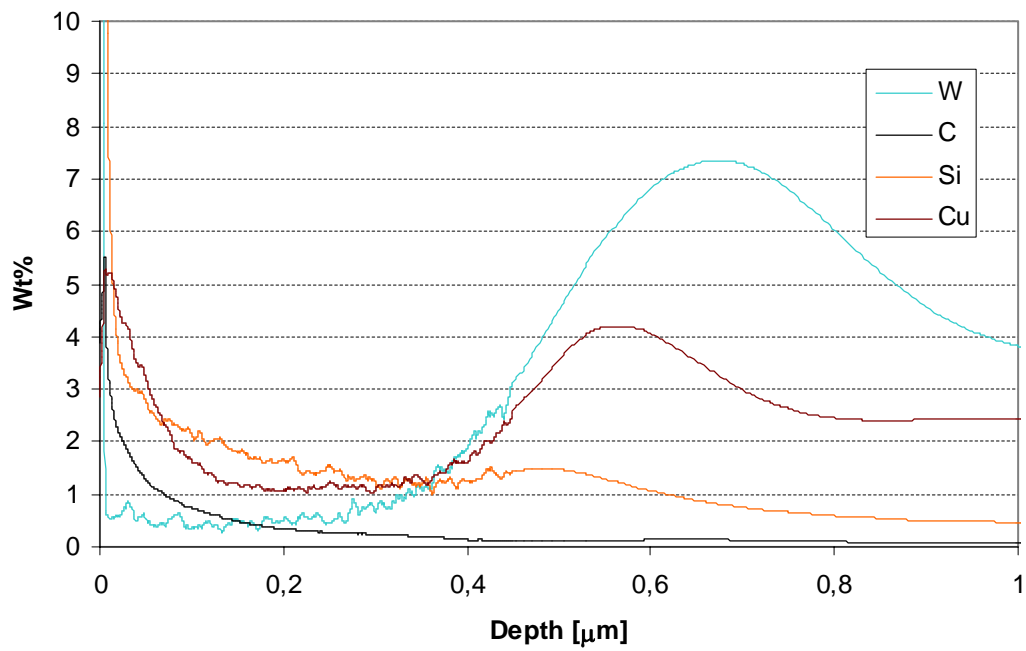
**Sanicro 25, 600°C - 1000 h, oxy**

**Sanicro 25, 600°C - 1000 h, oxy**


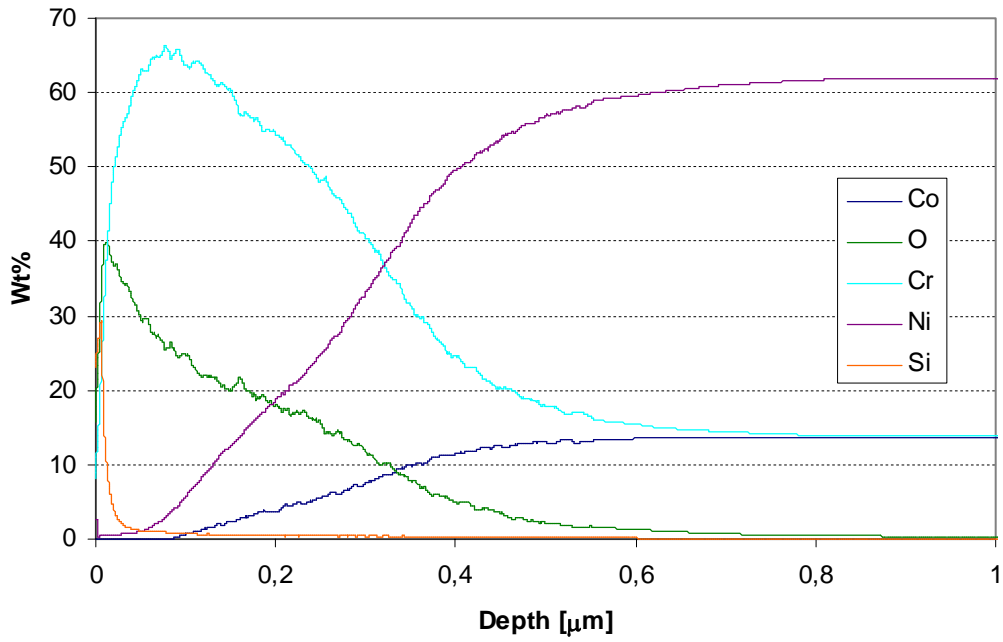
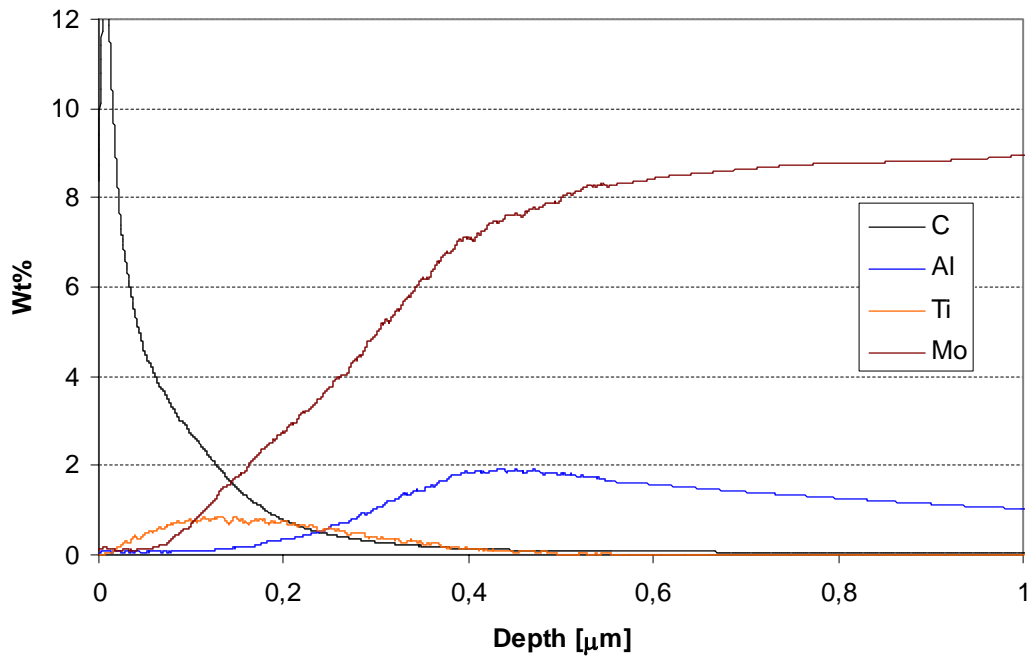
**Sanicro 25, 650°C - 500 h, air**

**Sanicro 25, 650°C - 500 h, air**


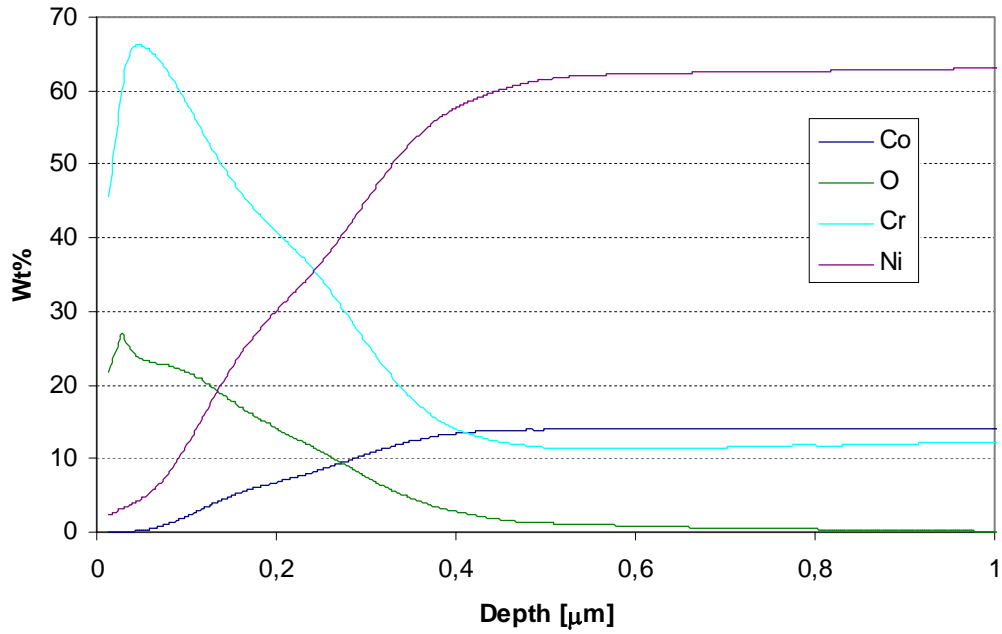
**Sanicro 25, 650°C - 500 h, oxy**



**Sanicro 25, 650°C - 500 h, oxy**



**A617, 650°C - 500 h, air**

**A617, 650°C - 500 h, air**


**A617, 650°C - 500 h, oxy**

**A617, 650°C - 500 h, oxy**
